Modeling and experimental verification of the dead metal zone for cutting force prediction in micro milling

Bowen Song
tianjin university
xiubing jing (jingxiuping@tju.edu.cn)
tianjin university
Jian Xu
tianjin university
Fujun Wang
tianjin university
Huaizhong Li
tianjin university

Research Article

Keywords: Micro cutting, dead metal zone, Cutting force, Separation point

Posted Date: February 24th, 2021

DOI: https://doi.org/10.21203/rs.3.rs-250268/v1

Modeling and experimental verification of the dead metal zone for cutting force prediction in micro milling

Bowen Song[1], Xiubing Jing[1*], Jian Xu[1], Fujun Wang[1], Huaizhong Li[2]

[1]Key Laboratory of Equipment Design and Manufacturing Technology, School of Mechanical Engineering, Tianjin University, Tianjin 300072, China

[2]Griffith School of Engineering, Gold Coast campus, Griffith University, QLD 4222, Australia

Abstract

In micro-cutting process, ploughing phenomenon occurring due to the dead metal zone (DMZ) leads to substantial ploughing force resulting in an obvious contribution to the total cutting force. To improve accuracy of the cutting force predicted, this paper aimed to explore the DMZ geometry related to the cutting depth and tool edge radius and thereof effect on cutting force. The prominent contribution of this research is to establish a new DMZ model by employing the slip-line field theory of the plastic formation. Based on the proposed model, DMZ are divided into shearing-dominated, mixed shearing and ploughing, and pure ploughing according to the minimum uncut chip thickness (MUCT). It is firstly proposed that the inner vertex of DMZ is the separation point of shearing effect and ploughing effect during metal cutting. The shape of the DMZ is theoretically calculated by an analytical way and verified by the simulation software. Finally, a cutting force model including shear force and ploughing force is established and verified by a series of experiments. The predicted cutting forces show remarkable agreement with those measured. The result proves that the separation point model is correct and can effectively demonstrate the ploughing force to accurately predict cutting force.

Keywords: Micro cutting; dead metal zone; Cutting force; Separation point.

*** Corresponding author:**

Dr. Xiubing Jing, Mechanical Engineering, Tianjin University, Tianjin, China, Email: jingxiuping@tju.edu.cn

Dr. Huaizhong Li, School of Engineering and Built Environment, Gold Coast campus, Griffith University, QLD 4222, Australia, Email: h.li@griffith.edu.au

1 Introduction

With the progress of modern manufacturing technology, the demand for micro-components in aviation, medical, electronics and other fields is gradually increasing. The flourish of micro-cutting technologies has greatly met the requirements for small parts in these fields. Among available micro-machining technologies, micro-milling possessing some advantages of high precision, high efficiency and low cost has been widely used in contemporary micro-machining[1]. There is an arc at the tool edge as shown Fig. 1 (a) [2], the tool cannot be treated as completely sharp, which led to the simultaneous presence of shearing and ploughing during micro-machining process. Some metal is detained nearby the tool edge named as dead metal zone (DMZ) which leads to ploughing and substantially affects the machining performance [3]. Ozturk and Altan [4] found a triangle-shaped zone existing in the front of the rounded tool edge in experiments (as shown in Fig. 1 (b)). In this study, it was also found that the material in this zone almost remained static through finite element simulation (as shown in Fig. 1 (c)). Chips are incompletely sheared and partially ploughed due to the effect of DMZ, which leads to material around the tool edge excessive plastic deformed. Moreover, the shearing and ploughing phenomena can be divided into three cases according to the value of cutting depth: shearing-dominated, mixed shearing and ploughing, and pure ploughing [4]. Firstly, the shearing effect is dominant when the cutting depth is large enough, which leads to produce complete chips and DMZ. Secondly, for case of the cutting depth beyond a given height related to the tool edge radius, the shearing and the ploughing effect occur simultaneously, which leads to the partly chip formation and a

variable DMZ generation. Thirdly, the cutting depth is less than a critical value named the minimum uncut chip thickness (MUCT), which leads to only ploughing occurring without chips formation. The size of DMZ can affect the cutting force, which is crucial for descripting the micro-cutting processes. However, the available cutting force models for micro-machining process believed that the shearing force and ploughing force are generated from uncut chip thickness and the extrusion /friction between the clearance face and surface generated [5], respectively. Actually, ploughing force is also related to the uncut chip thickness in practical micro-cutting process[6]. To improve accuracy of the cutting force predicted, it is important for investigating the size of DMZ and thereof on cutting force.

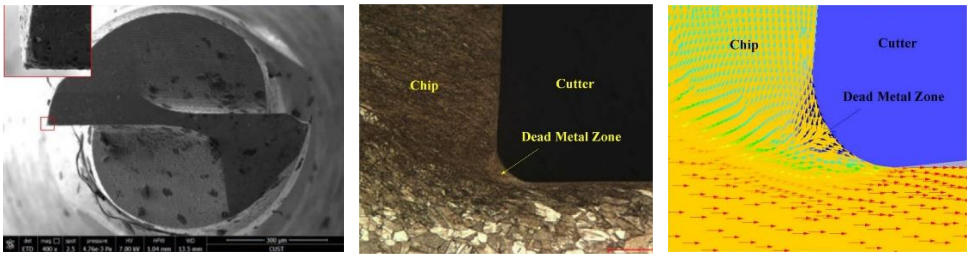

(a) (b) (c)

Fig. 1 (a) SEM of the tool tip [2]. (b) DMZ experimentally observed by Ozturk and Altan [4]. (c) DMZ simulated by the finite element with the diagrams of material flow velocity vector [3].

The slip line field theory has been widely employed in the prediction of cutting force by many researchers. Merchant [7] initially assumed the shear zone as a thin plane for establishing an orthogonal cutting model. Afterwards, Li and Schafer [8] assumed the workpiece as ideal rigid plasticity to establish a triangular slip line field model. To accurately predict the cutting force, Childs [9] introduced the elastic contact of the tool-chip to propose a new slip line field model. Furthermore, he compared the law of friction/stress models in the primary shear zone with those in secondary shear zone, and analyzed the temperature, strain and strain rate changes in the slip line field [10]. Oxley [11] presented a “parallel-side shear zone” model. Jin [12] considered the effect of rounded tool edge to propose a slip line field model for the micro-cutting process.

Above-mentioned cutting force models were established by employing slip line field theory and considered the material shear flow stress affected by the temperature, strain and strain rate. However, the DMZ can lead to the substantial ploughing force, which is critical to accurately predict cutting force in micro cutting process, there has been limited research on the effect of DMZ on cutting force.

Bissacco et al. [13] considered the influence of the rounded tool edge to develop a new cutting force model for micro end milling, which was based on an experimental investigation in orthogonal cutting. Yun et al. [14] presented a ploughing detection algorithm, and investigated the differences between ploughing and normal cutting by using the wavelet transformation of the cutting force signal in micro-milling processes. Jin [15] introduced the tool edge radius and chip size to present the prediction cutting force for orthogonal micro-cutting process, which also included in the tool run-out, dynamometer dynamics and trajectory of tool. Wan [16] proposed a new method of analyzing and predicting the position of the three vertices of the DMZ, theoretically determined all the separation points. Hu [17] proposed a modified analytical slip line field model to describe the cutting process with negative rake angle by using a chamfered edge tools, starting from the assumption of the material with rigid plastic deformation. Although the above-mentioned models have been studied on the ploughing effect or the dead metal zone, quantitative analysis and calculation have not been carried out by combining the slip line field with DMZ.

For accurately predicting the cutting force, this paper developed an improved the slip line field to calculate the three vertexes of DMZ. In this study, a new DMZ model based on the slip-line field theory is calculated by employing the plastic formation theory. It is firstly proposed that the inner vertex of DMZ is the separation point of shearing effect and ploughing effect during metal cutting. The shearing-dominated, mixed shearing and ploughing, and the pure ploughing models are established according to the cutting depth. The vertexes of DMZ are analytically estimated and verified by using FEM models. A

cutting force model including shearing force and ploughing force is established by considering the effect of DMZ. A series of experiments are conducted to verify the proposed method by the comparison predicted with measured cutting forces.

2 Development of the DMZ model

As described in introduction, the shearing and ploughing phenomena can be divided into three cases according to the value of cutting depth. The DMZ will be proposed as three cases according to the value of cutting depth in this section.

2.1 Shearing-dominated DMZ model

When the cutting depth is large enough, the cutting force is dominated by the shearing effect. In this case, the chip formation is relatively complete. To accurately predict the size of the DMZ in the cutting process, the first priority is to establish a complete slip line field model. In orthogonal micro-cutting metal process, the deformation region of material is composed by three areas: namely the primary and secondary shear zone, and tertiary zone. Fang [18] believed that the radius of tool edge can affect the main shear zone thickness and thereof on the slip line field shape, and initially proposed the slip line field shape. Jin [12] proposed an improved slip line field model considering the effect of temperature, strain and strain rate on the adhesion and sliding area, which assumed the shear stress along rake face and the tool-chip friction constant. In this section, the DMZ is embedded into the slip line field model proposed for calculating the size of shearing-dominated DMZ.

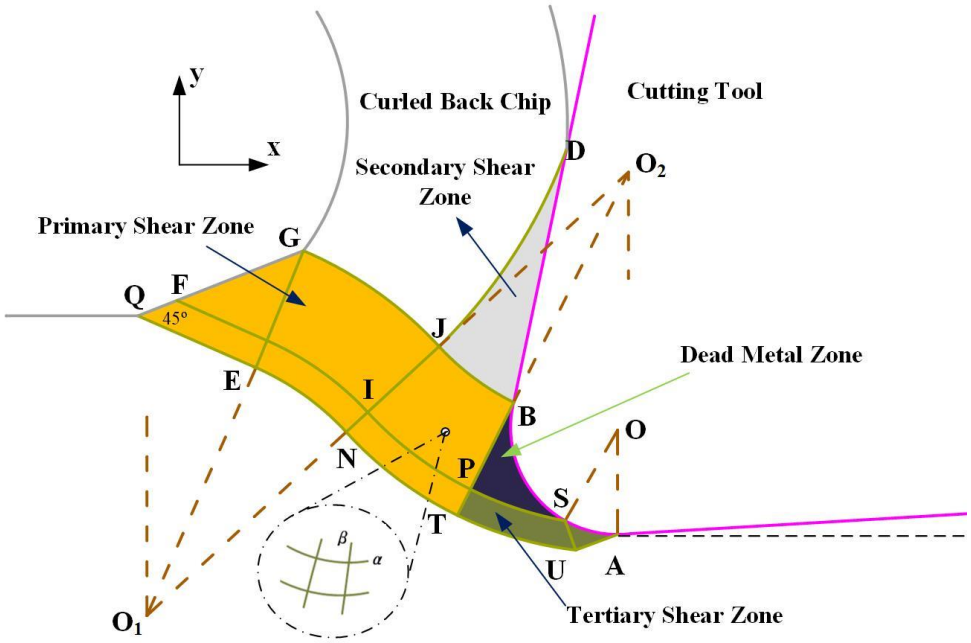

Fig. 2 Diagrams of slip line field for metal orthogonal micro-cutting

The slip line field considering the radius of tool edges is presented in Fig. 2. According to the Ref. [12], the shear zones are formed by α and β slip-lines perpendicular to each other. It is defined that counter-clockwise and clockwise couple are exerted the materials unit bounded by the slip-lines by the shear stress along the α and β slip-lines, respectively. Assuming the stress deformation and cutting conditions stable, it can be observed in Fig. 2 that the shear band is composed by four areas:

1) A polygonal area [GJBTNEQ] surrounded by slip lines is defined as the primary shear zone. Armarego and Brown [19] proposed that triangular QEG was the pre-flow effect in the shearing process. The slip line QG is the stress-free boundary. All slip lines in the triangle QEG intersect QG at a 45°. Green [20] proposed the tendency of GJNE area to be convex due to the rewinding effect of chips during metal cutting. The area JBTN is concave due to the friction between the chips and the tool rake face. The JBTN and GJNE areas are theoretically composed of radial lines and arcs, respectively.
2) A curved triangle BDJ is defined as the secondary shear zone. According to the Ref. [12], the direction of each slip line in this region is constant with rake angle

assuming the material already strain-hardened. The contact area of tool-chip can be divided into adhesion and sliding area. The chips in the sliding area slide with a constant coulomb friction coefficient, while, in the adhesion area, the ratio of friction stress to shear flow stress is constant. Both friction coefficient and adhesive shear stress are affected not only by tool and workpiece materials but also the surface roughness and temperature of rake face.

3) The polygon SAUTP is defined as the tertiary shear zone, which is mainly the ploughing effect resulting from the existence of rounded tool edge. Point P is the separation point formed during the cutting process. The material below the slip line PS will be squeezed and flow to the gap surface of the tool resulting in forming the so-called ploughing phenomenon.
4) The DMZ denoted by the BPS is located at the junction of the three main cutting deformation zones. The material above point B is mainly affected by the cutting force and slides upward to form chips, and the material below point S is mainly affected by the ploughing force to form a plough plane. In the BPS like-triangular area, the metal stagnation area called the DMZ is formed due to the simultaneous effect of adhesion of the tool, the shearing force, and the ploughing force.

2.1.1 Determination the position of separation point.

To calculate the size of DMZ during cutting process, the position of separation point B, P and S should be obtained. The position of point S can be obtained by finite element analysis and theoretical calculation methods. Recently, Wan [16] proposed a method to calculate the apex S of the DMZ by employing infinite shear strain theory to calculate the height of point S. However, this method did not establish a complete slip line field for calculation the DMZ during the micro-cutting process. In this study, to accurately determine the size of DMZ, a complete slip line field model should be established. As shown in Fig. 2, the separation points are located on the rounded tool edge. Therefore, the coordinate system should be established to describe the rounded tool edge and shown in Fig. 3.

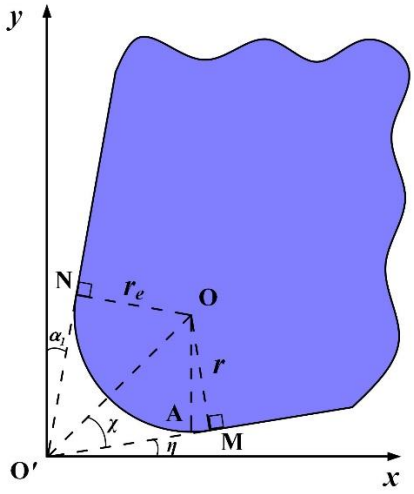

Fig. 3 The rounded tool edge in the coordinate system.

where η, α_1 and r_e are the relief angle, the rake angle, and the tool edge radius. χ is the inner angle of the triangle MOO'. Supposing the coordinates of point O and A as (O_x, O_y) and (A_x, A_y), the following formula can be geometrically derived:

$$\chi = \frac{90° - \alpha_1 - \eta}{2} \tag{1}$$

$$O_x = \frac{r_e}{\sin\chi}\cos(\chi + \eta) \tag{2}$$

$$O_y = \frac{r_e}{\sin\chi}\cos(\chi + \alpha_1) \tag{3}$$

The equation of the point (x, y) on the arc MN satisfies:

$$(x - O_x)^2 + (y - O_y)^2 = r_e^2 \tag{4}$$

The coordinates of point A are $(O_x, O_y - r_e)$.

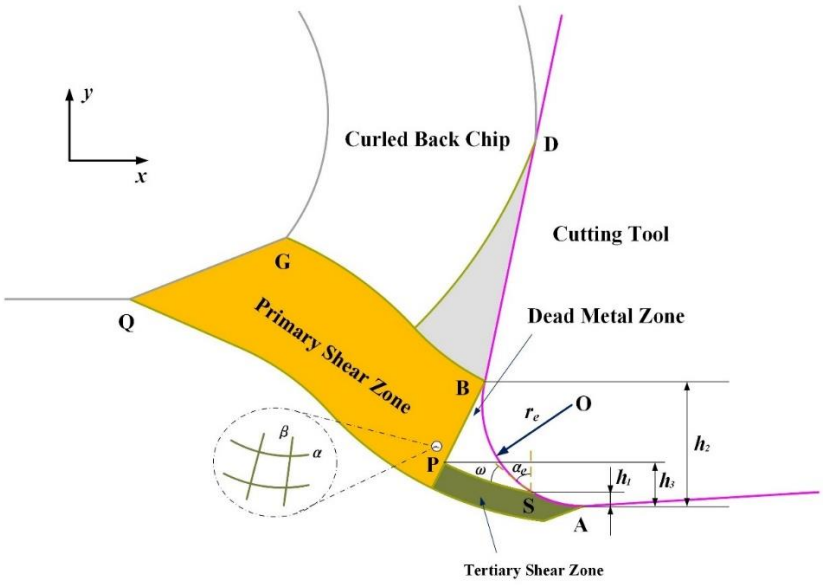

Fig. 4 Geometry of the DMZ

Fig. 4 shows the geometric relationship of the DMZ and the surrounding slip line field diagram. Where α_e is equivalent rake angle, h_1, h_2 and h_3 are the heights of DMZ's three vertexes S, B and P, respectively. ω is the angle between the tool boundary at point S and the α slip line, and can be calculated by using the friction coefficient of the workpiece-tool's contact surface. The coefficient of friction can be calculated by the ratio of shear stress to shear yield strength, and is difficult to accurately obtain due to the shear stress not directly measured during the micro-cutting process [21]. In this paper, employing the ultimate strain theory [22] and the calculation method of friction angle [23], a method for obtaining ω is proposed.

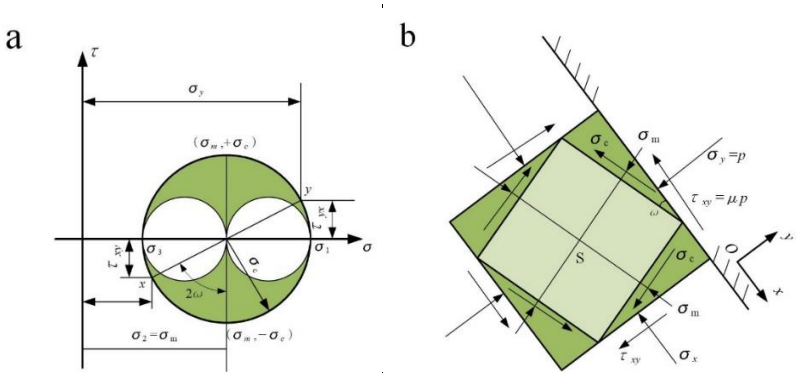

Fig. 5 (a) Mohr circle of stress (b) Stress conditions at S point

Referring to algorithm presented by Dewhurst [24] , the ω angle in the DMZ has the following formula:

$$\omega = 0.5\, cos^{-1}\left(\frac{\tau_{xy}}{k}\right) \tag{5}$$

where τ_{xy} is the shear stress in the τ direction as shown in Fig. 5(a). k refers to the flow stress corresponding to the actual stress required for plastic flow at a certain instant in the deformation process. Due to the work-hardening effect during the single stretching process, the plastic flow stress is increasing with increment deformation. Flow stress is a function related to speed and temperature deformation, and deformation degree. For the convenience of calculation, the flow stress is set as a constant with approximate equality to the yield limit σ_c.

Fig. 5 (b) presents the stress status at point S, which can deduce the following equations:

$$\begin{cases} \sigma_x = \sigma_m - \sigma_c \sin 2\omega \\ \sigma_y = \sigma_m + \sigma_c \sin 2\omega \end{cases} \tag{6}$$

where σ_x , σ_y, σ_m and σ_c are the x and y direction normal stress, the average stress and shear yield strength, respectively.

μ is the coefficient of friction at point S, then the following equation can be derived:

$$\begin{cases} \mu = \tan\beta \\ \tau_{xy} = \mu\sigma_y = \sigma_c \cos 2\omega \end{cases} \tag{7}$$

Where β is the friction angle of point S. Combining Eq. (6) with Eq.(7), it can be obtained that:

$$\mu\left(\sigma_m + \sigma_c \sin 2\omega\right) = \sigma_c \cos 2\omega \tag{8}$$

Employing the yield criterion of von Mises, the relationship between μ and ω can be finally deduced [16], as following Eq. (9).

$$\sqrt{3}\mu + \mu \sin 2\omega = \cos 2\omega \tag{9}$$

The ω can be calculated by Eq.(10):

$$\omega = \frac{\arcsin\dfrac{-\sqrt{3}\mu}{\sqrt{\mu^2+1}} + \arctan\mu}{2} \tag{10}$$

Some algorithms for the friction angle of some materials are proposed by Kaymakci and Altintas [23] through experimental analysis, as shown in Table 1.

Table 1: Formula for calculating friction angle of some materials.

Material	Al6061	Al7050-T7451	AISI-1045 Steel
Friction angle β (deg.)	20.835-4.901h-0.007v+0.291γ_n	25.877-1283h-0.007v +0.181γ_n	26.8-0.031v +11.77h

Where h, γ_n and v are uncut chip thickness in mm, normal rake angle in deg, and cutting velocity in m/min, respectively.

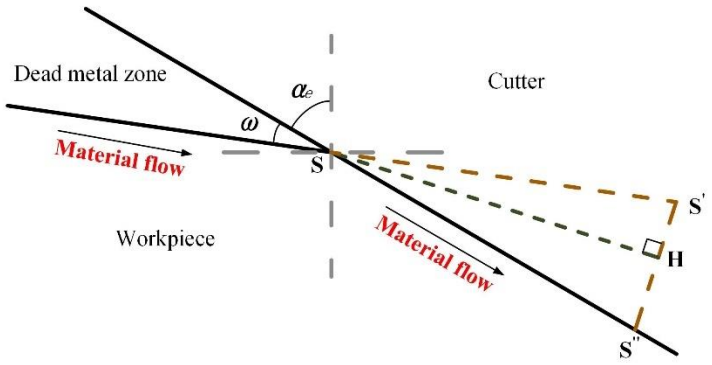

Fig. 6 Strain diagram of separation point S.

Fig. 6 presents the strain analysis diagram of point S. It can be seen that the workpiece is sheared by cutter lead to material fracturing and separating. The material below the point S is ploughed, while the material above the S point is very slowly moved and almost remains stagnant. As a separation point, the shear strain at point S approaches infinity. According to the infinite strain criterion for material stagnation proposed by M. Malekian [25]. Point S and point B can be seen as two stagnation point in chips formation process, and Eq. (11) can be derived from the infinite strain criterion [16].

$$\lambda=\frac{\overline{S'S''}}{\overline{SH}}=\frac{\overline{S'H}}{\overline{SH}}+\frac{\overline{S''H}}{\overline{SH}}=\cot\angle SS'S''+\cot\angle SS''S'=\infty \tag{11}$$

it can be obtained that:

$$\begin{aligned} &\angle SS'S'' = -180^\circ \text{ or } 0 \text{ or } 180^\circ \\ &\text{or} \\ &\angle SS''S' = -180^\circ \text{ or } 0 \text{ or } 180^\circ \end{aligned} \tag{12}$$

Based on the principle of maximum shear stress, Eq. (12) can be written as follows:

$$\angle SS'S'' = \varphi = 45^\circ - \left(\beta - \alpha_e\right) \tag{13}$$

where β is the friction angle, α_e is equivalent rake angle, which can be calculated from Eq.(14) and related to point S.

$$\alpha_e = -\left[90^\circ - \arccos\left(\frac{r_e - h_1}{r_e}\right)\right] \tag{14}$$

Where h_1 is defined geometrically in Fig. 4. In ΔSS'S'', the Eq. (15) can be obtained.

$$\angle SS''S' = 180^\circ - \angle SS'S'' - \angle S'SS'' = 180^\circ - \varphi - \omega \tag{15}$$

It can be derived from Eq.(6) to Eq.(15) that ∠SS'S'' and ∠SS''S' are functions of h_1. Combining Eq.(6) to Eq.(15), six solutions of h_1 can be obtained, while only two of them is valid. From a geometric view, the height of point B equal to h_2 corresponds to the solution with a larger value, while the height of point S equal to h_1 corresponds to the smaller solution.

From Fig. 4, it can be derived that the material above point P forms chips and the material below point P is squeezed by the DMZ to form the machined surface during the cutting progress. Therefore, the point P of the DMZ is regarded as the stagnation point of the ploughing effect and the shearing effect. To determine the position of point P, the established tool coordinate system shown in Fig. 3 should be used. Point A is set as the origin to establish a plane coordinate system. Combining the height of h_1 and h_2, the coordinates $\left(B_x, B_y\right)$ and $\left(S_x, S_y\right)$ of points B and S can be obtained from Eq. (4). As shown in Fig. 4, it can be concluded that BP is along the β slip line in the triangle BPS, and SP is along the α slip line. According to the slip line field theory [12], the α slip lines are perpendicular to the β slip lines, therefore, ∠BPS approximately satisfies:

$$\angle BPS = 90° \tag{16}$$

Assume the coordinates of point P as (P_x, P_y), it can be calculated by mathematical geometry from Eq. (17) and Eq. (18) in the following:

$$\begin{cases} \tan\left(\alpha+\omega+\dfrac{\pi}{2}\right)=\dfrac{S_y-P_y}{S_x-P_x} \\ \tan(\alpha+\omega)=\dfrac{B_y-P_y}{B_x-P_x} \end{cases} \tag{17}$$

$$\begin{aligned} P_x &= \frac{B_x\tan(\alpha+\omega)+S_x\cot(\alpha+\omega)-B_y+S_y}{\tan(\alpha+\omega)+\cot(\alpha+\omega)} \\ P_y &= \frac{B_y\cot(\alpha+\omega)+S_y\tan(\alpha+\omega)-B_x+S_x}{\tan(\alpha+\omega)+\cot(\alpha+\omega)} \end{aligned} \tag{18}$$

Combining the coordinates of points B, P and S, the size and shape of the triangle of the DMZ can be finally obtained.

2.2 Mixed shearing and ploughing DMZ model

2.2.1 Model expression

As shown in Fig. 7, when the cutting depth satisfied $h_1 < h < h_2$, where the h_1 and h_2 are calculated from section 2.1. For this case, discontinue chips can be generated during the cutting process resulting in the incomplete slip line field, which lacks the second deformation zone, so the slip line field model used in section 2.1 will no longer be suitable for this situation.

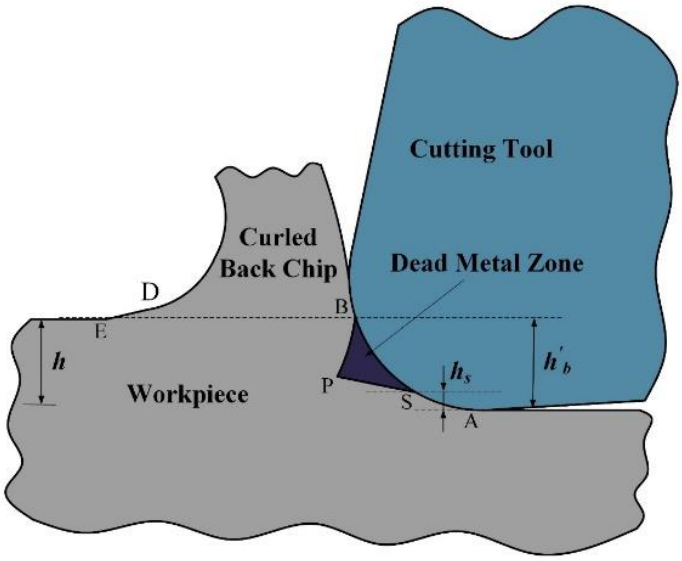

Fig. 7 Cutting state diagram when $h_1<h<h_2$

To establish a suitable DMZ model for this situation, the rounded cutting edge can be approximately regarded as negative rake angle chamfering tool. As described in the section 2.1, the point S in the DMZ is one of the separation points for ploughing during metal cutting. For this case, point S can be used as the base point to establish the slip line field model for incomplete DMZ. Therefore, the geometric size of the DMZ can be solved by employing the negative rake angle chamfering tool.

Fang [26] used a negative rake angle chamfering tool to model the DMZ in the slip line field during cutting progress. On this basis, considering the DMZ, Hu et al. [17] improved it and obtained a modified slip line field model, which was verified by the finite element method. As shown in Fig. 8, by considering DMZ and material pre-shear zone, this paper improved the above model and further presented a slip line field suitable for cutting depth satisfies the situation of $h_1 < h < h_2$.

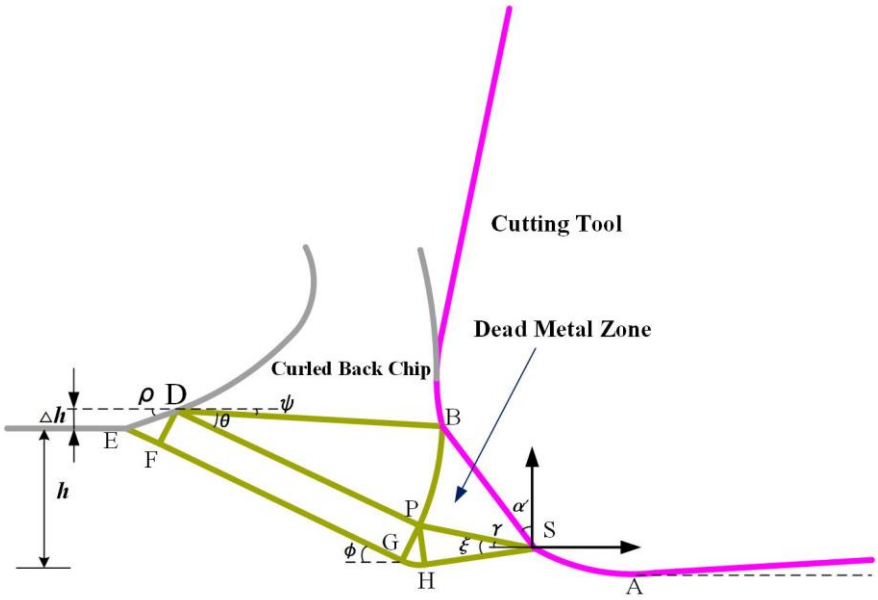

Fig. 8 Schematic diagram of improved slip line field model with chamfering tool

Fig. 8 presents the improved slip line field, namely the mixed shearing and ploughing DMZ model, which includes the following four main areas:

1) The first deformation zone is framed by DEFGHP. The equilateral right triangle area DEF represents the pre-cut zone, which is generated from the chips extruding and deforming before the workpiece material enters the main shear surface (DP).
2) The main slip line field is the sector area DBP. Through this area, the shearing speed in the first deformation zone gradually become the chip flowing speed.
3) The right triangle area PHS is the material area of the extruded workpiece, whose boundary is assumed to be an absolute straight line. There is no vertical flow of workpiece material at the DMZ-workpiece interface (PS), which is means that there is no material exchange between this zone and DMZ;
4) The triangle-like area PHS is the material retention area named DMZ, which is considered as a rigid body stably existing under the chamfered edge during cutting process. The point P is a stagnation point of the shearing effect and ploughing effect. Due to the smaller cutting depth, the formation of the DMZ is incomplete. According to the theory of maximum shear strain [25], the height of the upper vertex B of the DMZ is approximately the same as the depth of cut.

2.2.2 Model calculation

To ensure the continuity of the speed in the first deformation zone, THOMSEN [27] proposed that the rising height of the vertex D should be consistent with the rising height of the DMZ from the workpiece contact surface, which means that the vertical distance of DE from point D to the unprocessed surface should be equal to that of SP from point S to point P. The following relations can be obtained from Fig. 8:

$$\phi=\frac{\pi}{4}-\rho \tag{19}$$

$$\rho+\psi+\theta=\frac{\pi}{4} \tag{20}$$

where ϕ is the angle between EG and the horizontal direction. The inclination degree of the pre-shear zone's upper surface DE is represented by the bow angle ρ. ψ is the angle of the DB slip line in horizontal direction.

From geometric knowledge, the following formulas can be obtained:

$$\begin{aligned} l_{BD}&=l_{DP}=l_{FG}\\ l_{EF}&=l_{DF}=l_{GP}=l_{PH} \end{aligned} \tag{21}$$

$$l_{EF}=l_{PS}\sin\xi \tag{22}$$

where $l_{FG}, l_{AC}, l_{DP}, l_{AB}, l_{EF}, l_{PS}, l_{SB}, l_{BD}$ are the lengths of FG, AC, DP, AB, EF, PS, SB, BD, respectively. ξ is the friction factor angle on interface (PS) of the DMZ-workpiece. It can be derived from the slip line field modeling:

$$\frac{l_{EF}}{\sin 45^\circ}\sin\rho=l_{DB}\sin\psi \tag{23}$$

The coordinates of point S have been obtained in section 2.1. The relative position of point B can be obtained by combining the height of point B with the tool coordinate system in Fig. 3. As the DMZ modeling shown in Fig. 8, point S is set as the origin to establish a rectangular coordinate system, and the coordinates of point S and point B are (0, 0) and (B_x, B_y), respectively.

γ is the angle of the PS surface in horizontal direction and can be calculated as follows:

$$\gamma=90°-\alpha'-\omega \tag{24}$$

where ω at point S can be obtained from from Eq.(10) and the theoretical rake angle α' can be derived from Eq. (25):

$$\tan\alpha'=-\frac{B_x-S_x}{B_y-S_y} \tag{25}$$

Combining the cutting depth h and Eq.(4), coordinates (B_x, B_y) can be calculated. The height between point P and point S is defined as Δh, which is equal to the height between point D and point E as shown in Fig. 8. The coordinates of point P can be set as $\left(-\frac{\Delta h}{tan\gamma}, \Delta h\right)$, while point N is defined as the midpoint of line segment BP. The coordinates of point N is $\left(\frac{B_x-\frac{\Delta h}{tan\gamma}}{2}, \frac{B_y+\Delta h}{2}\right)$, while the coordinate of point D is $(D_x, B_y+\Delta h)$.

It can be derived that BP is perpendicular to DN from the geometric properties. The slopes of BP and DN are set as k_{BP} and k_{DN}, respectively. The following formulas can be obtained:

$$\begin{aligned} &k_{BP}\cdot k_{DN}=-1 \\ &\Rightarrow \\ &\frac{B_y-\Delta h}{\left(B_x+\frac{\Delta h}{\tan\gamma}\right)}\ \mathrm{g}\ \frac{B_y+\Delta h}{2\left(D_x-\frac{B_x+\Delta h/\tan\gamma}{2}\right)}=-1 \end{aligned} \tag{26}$$

From Eq.(26), it can be calculated that:

$$D_x=\frac{B_x^{\,2}-B_y^{\,2}+\Delta h^2-\left(\Delta h/\tan\gamma\right)^2}{2\left(B_x+\Delta h/\tan\gamma\right)} \tag{27}$$

Further, Eq.(28) can be derived:

$$\tan\phi=-\frac{D_y-P_y}{D_x-P_x}=\frac{2B_y\left(B_x+\Delta h/\tan\gamma\right)}{B_x^{\,2}-B_y^{\,2}+\Delta h^2-\left(\Delta h/\tan\gamma\right)^2+2B_x\Delta h/\tan\gamma} \tag{28}$$

By analyzing the geometric dimensions at ΔDEF, Eq.(29) can be obtained:

$$\frac{\Delta h}{\sqrt{2}\sin\left(\frac{\pi}{4}-\phi\right)}\sin\phi = h - B_y \tag{29}$$

Combining Eq. (28) with Eq. (29), Eq.(30) can be obtained as follows:

$$\begin{gathered}\left(h - B_y + h/\tan^2\gamma - 3B_y/\tan^2\gamma\right)\Delta h^2 + \\ \frac{2\left(h-B_y\right)\left(B_x - B_y\right)}{\tan\gamma}\Delta h + \left(h-B_y\right)\left(B_x{}^2 - B_y{}^2 - 2B_xB_y\right) = 0\end{gathered} \tag{30}$$

The value of Δh can be derived by solving Eq. (30), the coordinates of point P $\left(-\frac{\Delta h}{tan\gamma}, \Delta h\right)$ and D $\left(D_x, B_y + \Delta h\right)$ can be calculated.

ϕ can be derived from Eq. (28). The following relationship Eq. (31) can be obtained from the analysis of the slip line field size model in Fig. 8.

$$\sin\rho = \frac{\sin\gamma}{\sqrt{2}\sin\xi} \tag{31}$$

ρ can be calculated by Eq. (19), and ξ can be obtained from Eq. (31), so as to solve the model size of the slip line field.

2.3 Pure ploughing model

2.3.1 Model expression

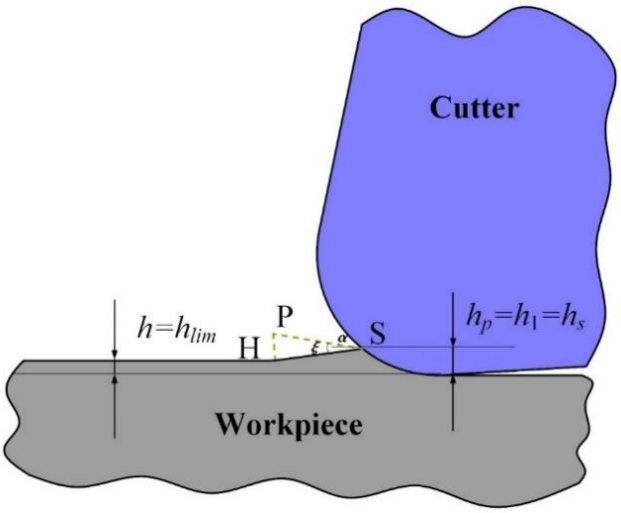

Fig. 9 Cutting diagram with cutting depth $h = h_{lim}$

Fig. 9 shows the cutting process with the cutting depth equal to the MUCT resulting in no chip formation, where the height of MUCT is set as h_{lim}, while h_p and h_s are defined as the plough thickness and the shear thickness, respectively. The lower apex of the DMZ is the separation point S, which is the same as the models established above. The DMZ is appearing when the material exceeds the point S.

2.3.2 Model calculation

According to the slip line model established in section 2.2, the triangle PSH shown in the Fig. 9 can be derived. h_{lim} can be calculated through solving the triangle size, as following.

$$h_{\lim} = h_1 - l_{sh}\sin\left(\xi - \gamma\right) \tag{32}$$

where l_{sh} is the length of SH that can be calculated by Eq.(33):

$$l_{sh} = l_{sp}\cos\xi \tag{33}$$

Combined with the calculation results from Eq.(30) to Eq.(33), the MUCT's height h_{lim} can be finally obtained.

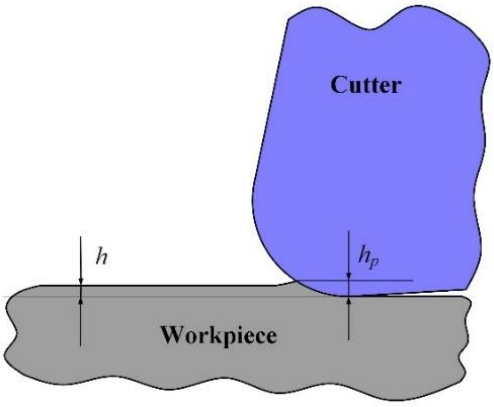

Fig. 10 Cutting diagram with depth of cut $h<h_{lim}$

When the cutting depth $h<h_{lim}$, only the ploughing effect occurring is shown in the Fig.10, which lead to the workpiece material squeezed to form a new surface. From the model establishment and analysis above, it can be approximated that there is a linear relationship between h and h_p. Therefore, the ploughing thickness h_p can be calculated

as follows:

$$h_p = \begin{cases} h_1, h = h_{\lim} \\ h + \dfrac{h}{h_{\lim}} l_{sh} \sin\left(\xi - \gamma\right), \quad h < h_{\lim} \end{cases} \tag{34}$$

3 Cutting force model

According to the slip line field model analysis above, it can be derived that during the cutting process, the plough thickness h_p can be expressed as：

$$h_p = \begin{cases} h_p, \ h \le h_{\lim} \\ h_3, \ h > h_{\lim} \end{cases} \tag{35}$$

while the shear thickness h_s can be expressed as：

$$h_s = \begin{cases} 0, \ h \le h_{\lim} \\ h - h_3, \ h > h_{\lim} \end{cases} \tag{36}$$

In our previous research [2], the cutting force model in micro milling has been partially studied, in which, the axial cutting depth is divided into units of equal thickness (dz). At any cutter rotation angle θ_m, when instantaneous uncut chip thickness $h(\theta_m)$ is less than h_{lim}, there is no shearing effect during the cutting process, only the ploughing force occurs. For a cutting unit dz, the cutting force generating from the k-th cutter edge are decomposed into the tangential force (dF_{tk}) and radial force (dF_{rk}), which can be given in Eq.(37):

$$\begin{cases} dF_{tk}\left(\theta_m\right) = k_{tp} \cdot h\left(\theta_m\right) \cdot dz \\ dF_{rk}\left(\theta_m\right) = k_{rp} \cdot h\left(\theta_m\right) \cdot dz \end{cases} \tag{37}$$

where k_{tp} and k_{rp} are the ploughing force coefficients in tangential direction and radial direction, respectively.

When the instantaneous uncut chip thickness is higher than h_{lim}, both shearing force and ploughing force are simultaneously existing during the cutting process. The cutting force given in Eq.(37) should be written by Eq.(38):

$$\begin{cases} dF_{tk}\left(\theta_m\right)=\left[k_{ts}+k_{tp}\right]\cdot h\left(\theta_m\right)\cdot dz \\ dF_{rk}\left(\theta_m\right)=\left[k_{rs}+k_{rp}\right]\cdot h\left(\theta_m\right)\cdot dz \end{cases} \tag{38}$$

where k_{ts} and k_{rs} are the shearing force coefficients in tangential direction and radial direction, respectively. The unit dz of the cutting depth can be written as:

$$dz=\frac{Rd\theta_m}{\tan\varsigma} \tag{39}$$

where R and ς are the tool radius and helix angle.

By conversing the tangential and radial force components into the Carter coordinate system, the cutting force can be calculated in the X and Y directions, which can be expressed by Eq.(40).

$$\begin{pmatrix} dF_{xk}\left(\theta_m\right) \\ dF_{yk}\left(\theta_m\right) \end{pmatrix}=\begin{pmatrix} -\cos\theta_m & -\sin\theta_m \\ \sin\theta_m & -\cos\theta_m \end{pmatrix}\begin{pmatrix} dF_{tk}\left(\theta_m\right) \\ dF_{rk}\left(\theta_m\right) \end{pmatrix} \tag{40}$$

By integrating the cutting force components obtained in Eq. (40), the cutting force generated by k-th flute in X and Y directions can be calculated by Eq.(41):

$$\begin{cases} F_{xk}\left(\theta_m\right)=\dfrac{R}{\tan\varsigma}\displaystyle\int_{\theta_l}^{\theta_u}\left[-dF_{tk}\left(\theta_m\right)\cos\theta_m-dF_{rk}\left(\theta_m\right)\sin\theta_m\right]d\theta_m \\ F_{yk}\left(\theta_m\right)=\dfrac{R}{\tan\varsigma}\displaystyle\int_{\theta_l}^{\theta_u}\left[dF_{tk}\left(\theta_m\right)\sin\theta_m-dF_{rk}\left(\theta_m\right)\cos\theta_m\right]d\theta_m \end{cases} \tag{41}$$

where θ_l and θ_u are the entry angle and exit angle of the flute, respectively. Finally, the total cutting force can be calculated by Eq. (42).

$$\begin{cases} F_x\left(\theta_m\right)=\displaystyle\sum_{k=1}^{K}F_{xk}\left(\theta_m\right) \\ F_y\left(\theta_m\right)=\displaystyle\sum_{k=1}^{K}F_{yk}\left(\theta_m\right) \end{cases} \tag{42}$$

where K is the number of teeth.

According to the Ref. [2], the cutting force coefficient can be fitted formula as a nonlinear function of the depth of cutting, as follows:

$$\begin{cases} k_{ts}=a_t\cdot h_s^{\,b_t} \\ k_{rs}=a_r\cdot h_s^{\,b_r} \end{cases} \tag{43}$$

the fitting formula of ploughing force is set by Eq.(44):

$$\begin{cases} k_{tp} = c_t \cdot h_p^{\,d_t} \\ k_{rp} = c_r \cdot h_p^{\,d_r} \end{cases} \tag{44}$$

The parameters in Eq.(43) and Eq. (44) obtaining by method of curve fitting are listed in the Table 2.

Table 2 : Parameters related to coefficients cutting force.[2]

a_t	b_t	c_t	d_t	a_r	b_r	c_r	d_r
744.420	-0.271	-8.855	69.377	21.073	0.957	-1.135	-1.243

4 Theory and simulation model analysis

To assess the applicability of the model established in section 2, multiple sets of FEM simulations were carried out to simulate the size of DMZ by using Deform 2D/3D software. The tool is defined as pure rigid material participating in heat transfer. In the meshing process, Arbitrary Lagrange Eulerian (ALE) adaptive method is used to avoid too much deformation of materials around the cutter. Both the room temperature and the initial temperature condition for tools and workpieces are set as 20° C. In this study, Al6061 is selected as the workpiece material, and the width and cutting speed are kept at 2.5 mm and 104.67 m/min, respectively. The workpiece only moves in the horizontal direction and is fixed in the vertical direction. In order to ensure the simulation accuracy and efficiency, the mesh refinement is performed on the tool edge as well as the workpiece.

Subsequently, FEM simulation is mainly performed in two situations: the one is set the cutting depth constant to simulate the shape of the DMZ by the simulation step changing. The other way is using the constant simulation step to simulate the shape of the DMZ with the cutting depth changing. The shape can be judged by measuring the height of the three vertices of the triangle in the DMZ as shown in the Fig.11, where (a) and (b) are simulation diagram and theoretical diagram, respectively. The geometric dimensions of the tool are shown in Table 3.

Table 3 Geometric dimensions of the tool.

Cutter no.	Radius（mm）	Tool edge radius (μm)	Rake angle (◦)	Relief angle(◦)	Material
1	0.6	5	5	5	WC
2	0.6	8	5	5	WC

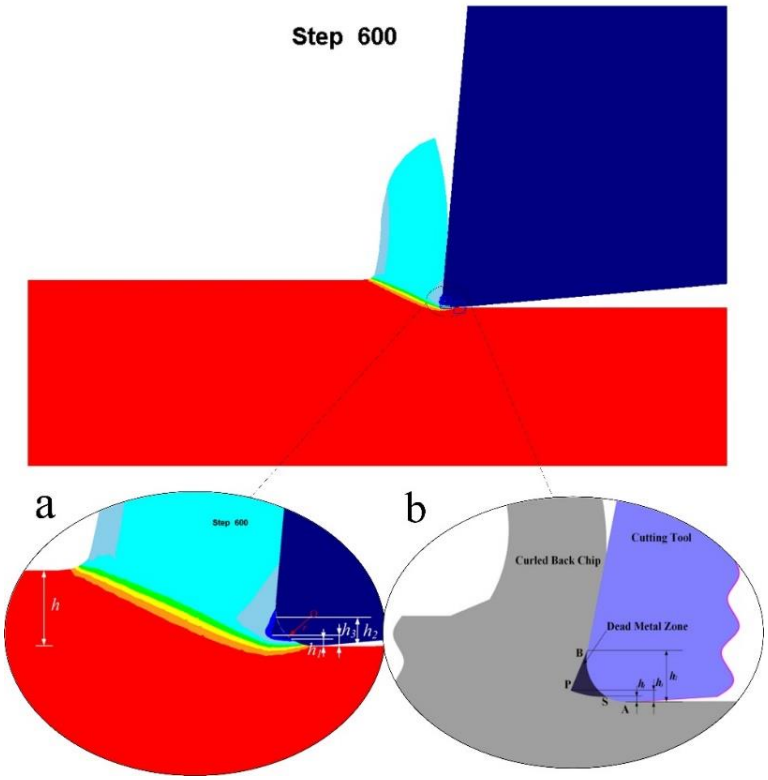

Fig. 11 Three vertices height of simulated DMZ (a) Simulation diagram (b) Theoretical diagram

Through simulation, the height of the triangle apex in the DMZ can be obtained under different cutting depths and different cutting steps. The specific conditions are presented in the Table 4.

Table 4 Experimental conditions.

Test no.	Material	Cutter no.	simulation step	cutting depth（mm）
1	Al6061	1	200	15

2	Al6061	1	400	15
3	Al6061	1	600	15
4	Al6061	1	800	15
5	Al6061	1	800	0.65
6	Al6061	1	800	2
7	Al6061	1	800	4
8	Al6061	1	800	8
9	Al6061	1	800	16
10	Al6061	2	800	2
11	Al6061	2	800	4
12	Al6061	2	800	8
13	Al6061	2	800	16

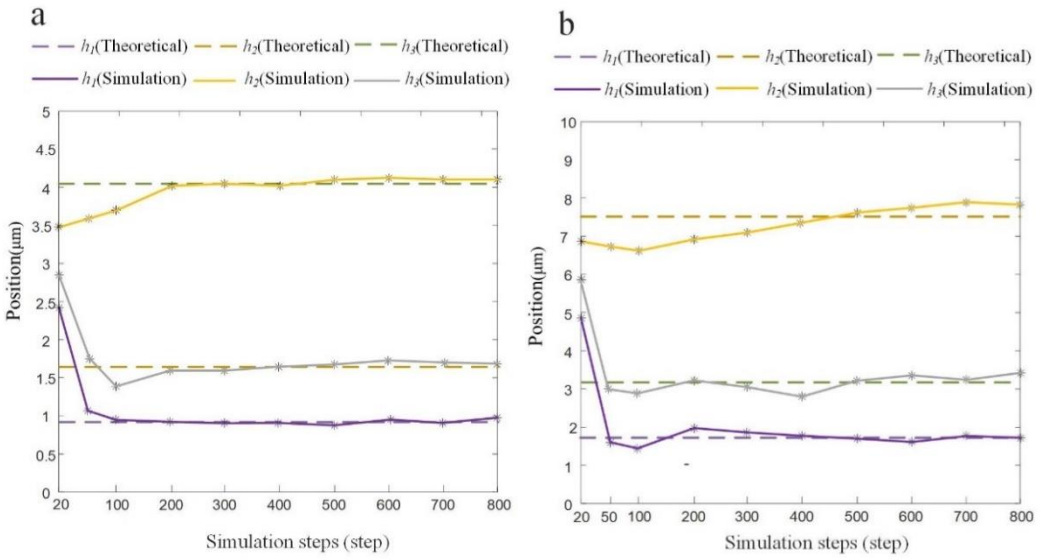

Fig. 12 Comparison height acquired for separation points' by simulation with that of theoretically predicted under the condition at (a) r_e = 5 μm and (b) r_e= 8 μm.

Fig.12 shows the comparison of the height of separation points theoretically predicted and that of numerically simulated in the DMZ with (a) r_e = 5 μm and (b) r_e= 8 μm, while the cutting depth is set as 16 μm. It is worth emphasizing that when the step size is higher than 200 steps, the size and shape of the dead model zone are approximately no longer changed. It can be seen that the DMZ is immediately generated once the tool edge touching the workpiece, which can be explained that the cutting depth meets the conditions for complete chip formation. In the first, due to only the upper half of the

tool edge touching the workpiece, the DMZ is located at a higher position, and the shape is not regular. When the rounded tool edge fully engages into the workpiece, the complete DMZ is formed. With the cutting process going on, the shape of the DMZ remains basically stable. The height of the three vertices of the DMZ obtained by simulation is compared with the theoretical position obtained by the previous calculation shown in Fig.12. As the shape of the DMZ becomes basically stable, the fitting error between the simulated position and the theoretical position is within 10%, which proves the theoretical modeling of the DMZ's correctness.

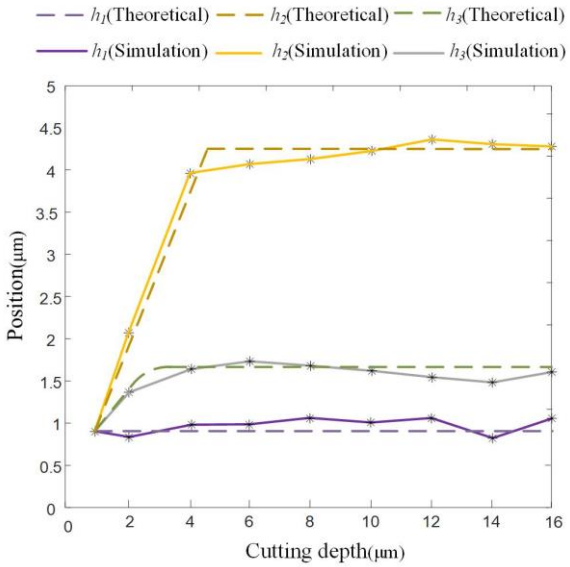

Fig. 13 Comparison height acquired for separation points' by simulation with that of theoretically predicted at different uncut chip thickness with r_e = 5 μm

Fig.13 shows the comparison separation points' height acquired by simulation with that of theoretically predicted at different uncut chip thickness with r_e = 5 μm. It can be observed from Fig.13 that the cutting process is dominated by ploughing effect resulting in no DMZ formed for the case of the cutting depth less than the MUCT, and the DMZ begins to form for case of the cutting depth higher than the MUCT. The height h_1 of point S in the DMZ remains basically unchanged while the height of h_2 point B rises rapidly, and basically remain stable when it reaches to a certain height. The separation point P of material ploughing and shearing, also has the same characteristics. When the

shape of the DMZ becomes basically stable, it can be seen that the fitting error between the simulated position and the theoretical position is within 10 %, which proves the theoretical modeling of the DMZ's correctness.

These simulation results indicate that the geometry of the DMZ is substantially affected by the radius of tool edge, which means that the radius of tool edge is directly engaged in the formation of DMZ and effects thereof on the shape of DMZ. However, once the cutting depth ensures that the chips can reach the height of h_2, it will not affect the size of DMZ.

5 Experimental verification

To verify the correctness of the model presented in Section 2, a train of micro- milling experiments were carried out on the 3-axis micromachining center developed in-house with 0.5 μm resolution in each direction as shown in Fig.14. In this experiment, the test uses Al6061 as the material of the workpiece with the size of 60 mm × 10 mm × 3 mm. The cutter with two flutes by superfine tungsten steel with TiAIN coated is used. The helix angle and tool radius are 35° and 0.8 mm, respectively. Kistler 9317B dynamometer is used to measure the cutting force, whose sensitivity is 25.65 pC/N and 25.37 pC/N in the X and Y directions, respectively. To remove high-frequency noise in the experiments, the cutting force signals are smoothed by a low-pass filter, whose cut-off frequency is set as 800 Hz. The experimental conditions and parameters are summarized in Table 5.

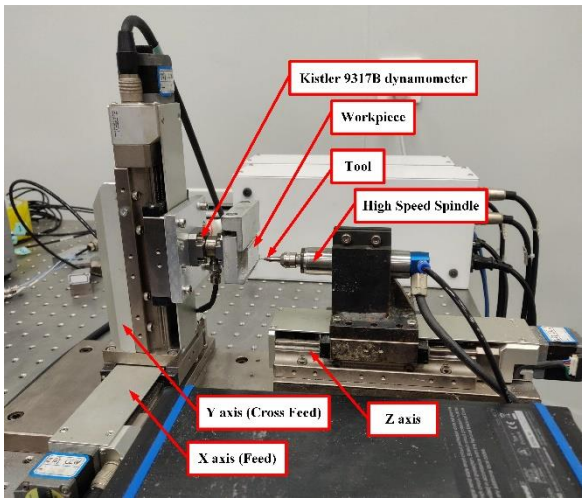

Fig. 14 the 3-axis micromachining center

Table 5 Conditions and parameters in cutting experiments.

Test no.	Radius （mm）	Tool edge radius(μm)	Rake angle(°)	Axial depth of cut(μm)	Feed rate (μm /tooth)	Spindle speed (rpm)
1	0.3	5	10	50	0.8	4000
2	0.3	5	10	50	2	4000
3	0.3	5	10	50	4	4000
4	0.3	5	10	50	8	4000
5	0.3	5	10	50	16	4000

Table 6 physical properties of Al6061.

Material	Poisson's Ratio	Young's Modulus (GPa)	Density (g/cm^3)	Melt Temperature （° C）	Expansion Coefficient ($/10e\text{-}6/^{\circ}C^{-1}$)	Specific Heat (J/ (kg·C))	Heat Conductivity (W/ (m·C))
Al6061	0.33	69	2.70	1530~1650	23.4	580	10.4

The material selected for this experiment is Al6061, whose physical properties are shown in Table 6. The workpiece is treated as elastic-plastic behavior represented by Johnson-Cook material model and the flow stress has been calculated by Eq.(45) according to the Ref. [28]:

$$\sigma=\left[A_1+B_1\varepsilon^n\right]\left[1+C_1\ln\frac{\dot{\varepsilon}}{\dot{\varepsilon}_0}\right]\left[1-\left(\frac{T-T_{room}}{T_{melt}-T_{room}}\right)^m\right] \tag{45}$$

where $\varepsilon, \dot{\varepsilon}$ and $\dot{\varepsilon}_0$ are equivalent plastic strain, strain rate of equivalent plastic and reference plastic, respectively. T, T_{melt} and T_{room} are the temperature of work, the material melting and the room, respectively. According the Ref. [29], n, m, A_1, B_1 and C_1 are the material constants in constitutive relationship of the Johnson–Cook, which are list in Table 7.

Table 7 Al6061 constants for Johnson–Cook model.

A1 [MPa]	B1 [MPa]	C_1	M	n	$\dot{\varepsilon}_0$	T_{melt} [K]	T_{room} [K]
225	184	0.0396	2.19	0.157	$162s^{-1}$	633	283.4

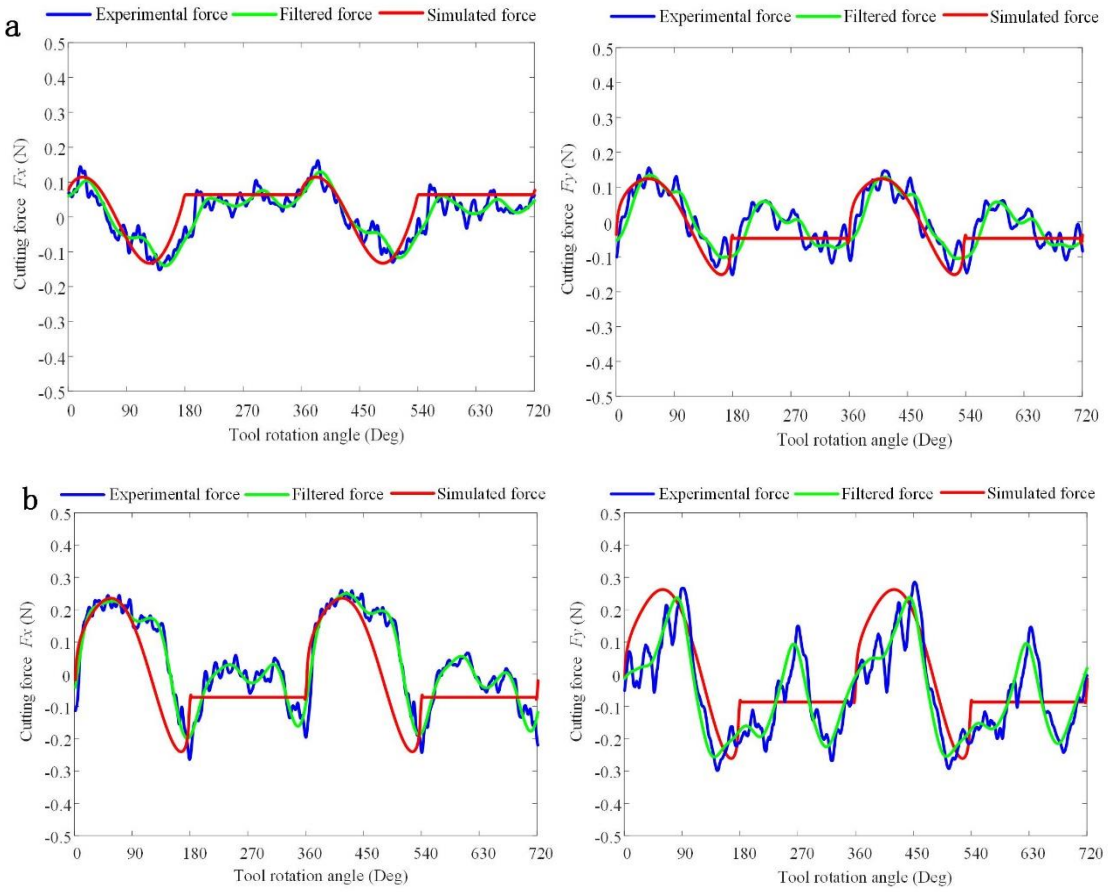

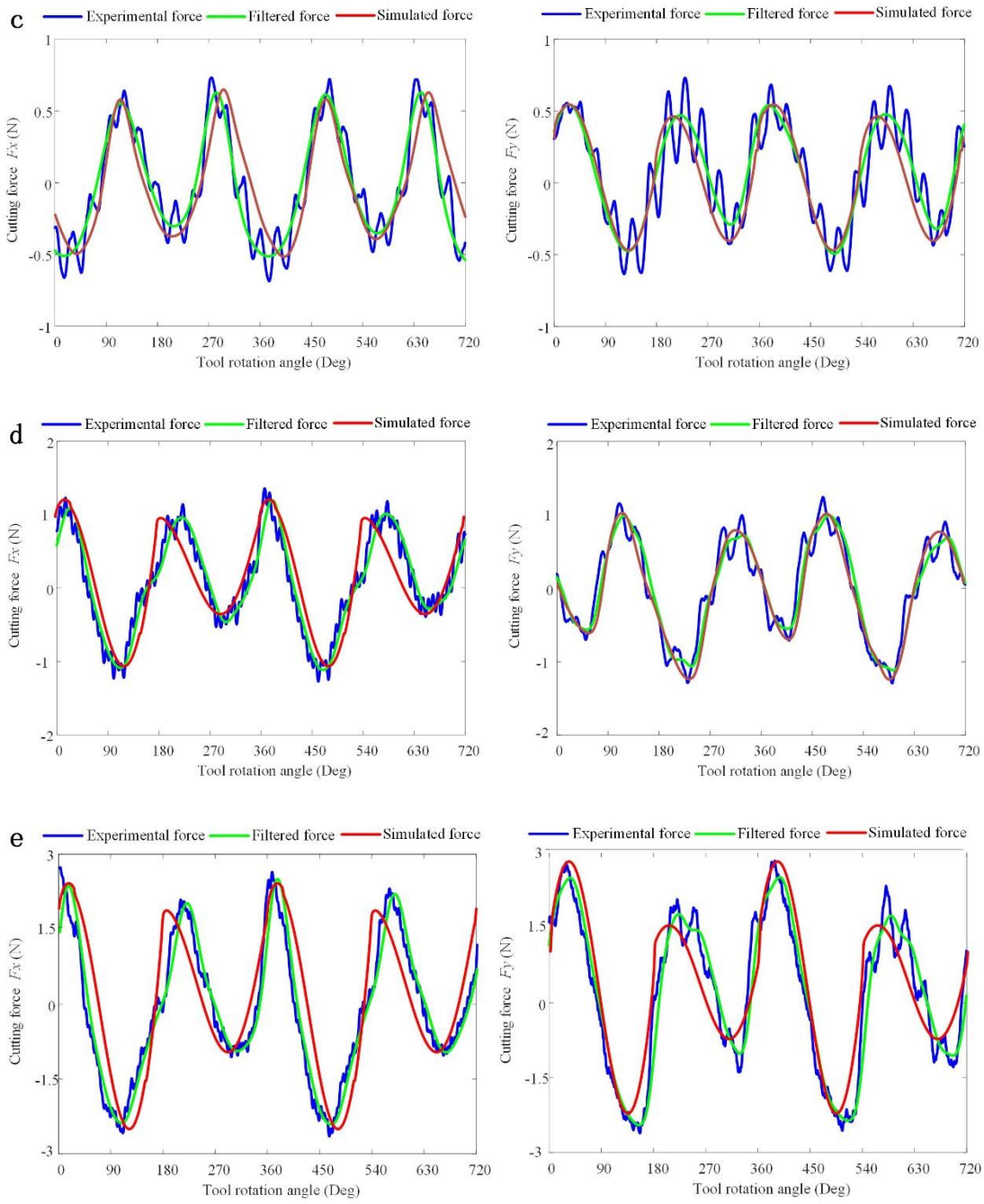

Fig. 15 Comparison cutting force predicted with that of measured in micro/macro milling process (a) Test 1, (b) Test 2, (c) Test 3, (d) Test 4, (e) Test 5.

Fig. 15 presents the differences between the cutting force predicted and that of experimentally measured in the X and Y directions for micro milling process. Among these comparisons, Fig.15 (a) presents the results at 0.8 μm feed per tooth, which is approach to or less than the value of MUCT lead to the pure ploughing phenomenon

occurring during the micro-milling process, therefore the ploughing force is relatively stable. The experimental results and the filtered simulation results have an error within 10%, which proves the correctness of the plough force modeling.

Fig.15 (b) and Fig.15 (c) show the experiments where the feed per tooth is 2 μm and 4 μm, respectively, which can present the phenomenon of mixed ploughing and shearing in micro-milling process. In the cutting process corresponding to Fig.Fig. 15 (b), the feed per tooth is higher than the value of MUCT, which lead to the dominant share of ploughing force. However, due to the addition of shear force, it is also quite different from the pure ploughing force in Fig. 15 (a). Among the cutting forces in Fig. 15 (c), the feed per tooth is approach to that of macro milling resulting in the dominant shearing force, and the experimental results fit well with the filtered simulation results due to the effect of shearing force on cutting force almost ignored. It is worth noted that a minor fluctuation is appearing in the measured cutting force, this phenomenon is due to the slight vibration occurring during the micro-milling process. However, the peak value and wave of the measured force can not be substantially affected by these shapes of fluctuations, and the collected force still matches the predicted cutting force well in terms of shape, peak value, and global change trend.

Fig.15 (d) and Fig.15 (e) correspond to 8 μm microns and 16 μm per tooth respectively. In this case, the share of shear force dominates most of the cutting force. From the comparisons of the measured cutting force and that of simulated in the figure, it can be obtained that the size of DMZ and separation point proposed in the previous chapters are reliable for the cutting force prediction.

It is worth noting that there usually exists the phenomenon of the tool run-out and the eccentricity problems during the micro-milling process. This leads to the observation in the image: although the experimental data matches the predicted cutting force well in terms of shape, peak value and global change trend, there will still be some certain

errors. These issues will continue to be studied in subsequent research.

6 Conclusions

In the metal cutting process, the cutting force mainly includes shearing force and ploughing force, which should be accurately determined by the separation point in the process of modeling the cutting force. In this study, based on the plastic forming theory, the DMZ modeling is added to the slip line field model. For different cutting depths, an improved slip line field model is established, including the shearing-dominated DMZ model, mixed shearing and ploughing DMZ model and pure ploughing model.

It is also proposed that in the shearing-dominated DMZ model and mixed shearing and ploughing DMZ model, the inner vertex of the triangle of the DMZ is the separation point of ploughing and shearing during metal cutting. One kind of tool coordinate system model is established. The theoretical calculation method for the size of the DMZ model in the slip line field is proposed, and the size of the DMZ and the minimum uncut thickness are determined by this method. The influence of cutting depth and simulation step length on the size of DMZ is simulated by the Deform 11.0 software. The good agreement between the simulation results and the theoretical prediction values proves the correctness of the theoretical modeling.

Based on the established DMZ model, the previous cutting force modeling was improved. For different uncut chip thicknesses, the shearing force and the ploughing force are calculated separately. Through simulation and experiments, the accuracy of pure ploughing force modeling is verified. According to the analysis of the established cutting force model, as the cutting depth growing, the ploughing force gradually increases. Until the cutting depth reaches the MUCT, the DMZ begins to form. And the separation point between the ploughing effect and the shearing effect began to appear. The shear force starts to increase and keeps growing as the cutting depth rises while the

ploughing force also continues to increase until a complete DMZ is formed. Then the ploughing force will remain stable and stop increasing.

A train of experimental milling were performed to verify the proposed model with different cutting conditions. The measured cutting forces show a great agreement with that of predicted, which proves that the separation point proposed is effective to distinguish the ploughing phenomenon during metal cutting.

Funding

This research is supported by Science & Technology Commission of Tianjin Municipality (Grant no 19PTZWHZ00010), National Key R&D Program of China (nos. 2017YFE0112100，and 2019YFB1301902), National Natural Science Foundation of China (Grant no. 51675376).

Authors' contributions

Bowen Song and Xiubing Jing contributed to the conceptualization, writing and editing. Jian Xu and Huaizhong Li contributed to the methodology. Fujun Wang provided resources.

Compliance with ethical standards

Conflict of interest The authors declare that they have no conflicts of interest.

Ethical approval Not applicable.

Consent to participate Yes, consent to participate from all the authors.

Consent to publish Yes, consent to publish from all the authors.

References

[1] K. Venkata rao, A study on performance characteristics and multi response

optimization of process parameters to maximize performance of micro milling for Ti-6Al-4V, J. Alloys Compd. 781 (2019) 773–782.
[2] X. Jing, R. Lv, Y. Chen, Y. Tian, H. Li, Modelling and experimental analysis of the effects of run out, minimum chip thickness and elastic recovery on the cutting force in micro-end-milling, Int. J. Mech. Sci. 176 (2020) 105540.
[3] K.V. Rao, B.H. Babu, V.U. Vara Prasad, A study on effect of dead metal zone on tool vibration, cutting and thrust forces in micro milling of Inconel 718, J. Alloys Compd. 793 (2019) 343–351.
[4] S. Ozturk, E. Altan, A slip-line approach to the machining with rounded-edge tool, Int. J. Adv. Manuf. Technol. 63 (2012) 513–522.
[5] M.A. Câmara, J.C.C. Rubio, A.M. Abrão, J.P. Davim, State of the Art on Micromilling of Materials, a Review, J. Mater. Sci. Technol. 28 (2012) 673–685.
[6] H. YUAN, M. WAN, Y. YANG, Design of a tunable mass damper for mitigating vibrations in milling of cylindrical parts, Chinese J. Aeronaut. 32 (2019) 748–758.
[7] M.E. Merchant, Mechanics of the metal cutting process. I. Orthogonal cutting and a type 2 chip, J. Appl. Phys. 16 (1945) 267–275.
[8] E.H. Lee, The theory of plasticity applied to a problem of machining, ASME J. Appl. Mech. 18 (1951) 405.
[9] T.H.C. Childs, Elastic effects in metal cutting chip formation, Int. J. Mech. Sci. 22 (1980) 457–466.
[10] T.H.C. Childs, MATERIAL PROPERTY NEEDS IN MODELING METAL MACHINING, Mach. Sci. Technol. 2 (1998) 303–316.
[11] P.L.B. Oxley, M.C. Shaw, Mechanics of Machining: An Analytical Approach to Assessing Machinability, J. Appl. Mech. 57 (1990) 253.
[12] X. Jin, Y. Altintas, Slip-line field model of micro-cutting process with round tool edge effect, J. Mater. Process. Technol. 211 (2011) 339–355.
[13] G. Bissacco, H.N. Hansen, J. Slunsky, Modelling the cutting edge radius size effect for force prediction in micro milling, CIRP Ann. - Manuf. Technol. 57 (2008) 113–116.
[14] H.T. Yun, S. Heo, M.K. Lee, B.K. Min, S.J. Lee, Ploughing detection in micromilling processes using the cutting force signal, Int. J. Mach. Tools Manuf. 51 (2011) 377–382.
[15] X. Jin, Y. Altintas, Prediction of micro-milling forces with finite element method, J. Mater. Process. Technol. 212 (2012) 542–552.
[16] M. Wan, D.Y. Wen, Y.C. Ma, W.H. Zhang, On material separation and cutting force prediction in micro milling through involving the effect of dead metal, Int. J. Mach. Tools Manuf.,146 (2019) 103452.
[17] C. Hu, K. Zhuang, J. Weng, X. Zhang, Thermal-mechanical model for cutting with negative rake angle based on a modified slip-line field approach, Int. J. Mech. Sci. 164 (2019) 105167.
[18] N. Fang, P. Dewhurst, Slip-line modeling of built-up edge formation in machining, Int. J. Mech. Sci. 47 (2005) 1079–1098.

[19] E.J.A. Armarego, R.H. Brown, The machining of metals, PRENTICE-HALL INC, ENGLEWOOD CLIFFS, N. J., 1969, 437 P. (1969).
[20] A.P. Green, On the use of hodographs in problems of plane plastic strain, J. Mech. Phys. Solids. 2 (1954) 73–80.
[21] Altintas Y , Author, Ber AA , Reviewer, Manufacturing Automation: Metal Cutting Mechanics, Machine Tool Vibrations, and CNC Design, Appl. Mech. Rev. 54 (2001) B84–B84.
[22] M. Malekian, M.G. Mostofa, S.S. Park, M.B.G. Jun, Modeling of minimum uncut chip thickness in micro machining of aluminum, J. Mater. Process. Technol. 212 (2012) 553–559.
[23] M. Kaymakci, Z.M. Kilic, Y. Altintas, Unified cutting force model for turning, boring, drilling and milling operations, Int. J. Mach. Tools Manuf. 54–55 (2012) 34–45.
[24] P. Dewhurst, A general matrix operator for linear boundary value problems in slip-line field theory, Int. J. Numer. Methods Eng. 21 (1985) 169–182.
[25] M. Malekian, M.G. Mostofa, S.S. Park, M.B.G. Jun, Modeling of minimum uncut chip thickness in micro machining of aluminum, J. Mater. Process. Technol. 212 (2012) 553–559.
[26] N. Fang, Tool-chip friction in machining with a large negative rake angle tool, Wear. 258 (2005) 890–897.
[27] E.G. Thomsen, A.G. MacDonald, S. Kobayashi, Flank Friction Studies With Carbide Tools Reveal Sublayer Plastic Flow, J. Eng. Ind. 84 (1962) 53–62.
[28] P. Rodríguez, J.E. Labarga, Tool deflection model for micromilling processes, Int. J. Adv. Manuf. Technol. 76 (2014) 199–207.
[29] M. Scapin, A. Manes, Behaviour of Al6061-T6 alloy at different temperatures and strain-rates: Experimental characterization and material modelling, Mater. Sci. Eng. A. 734 (2018) 318–328.

Figures

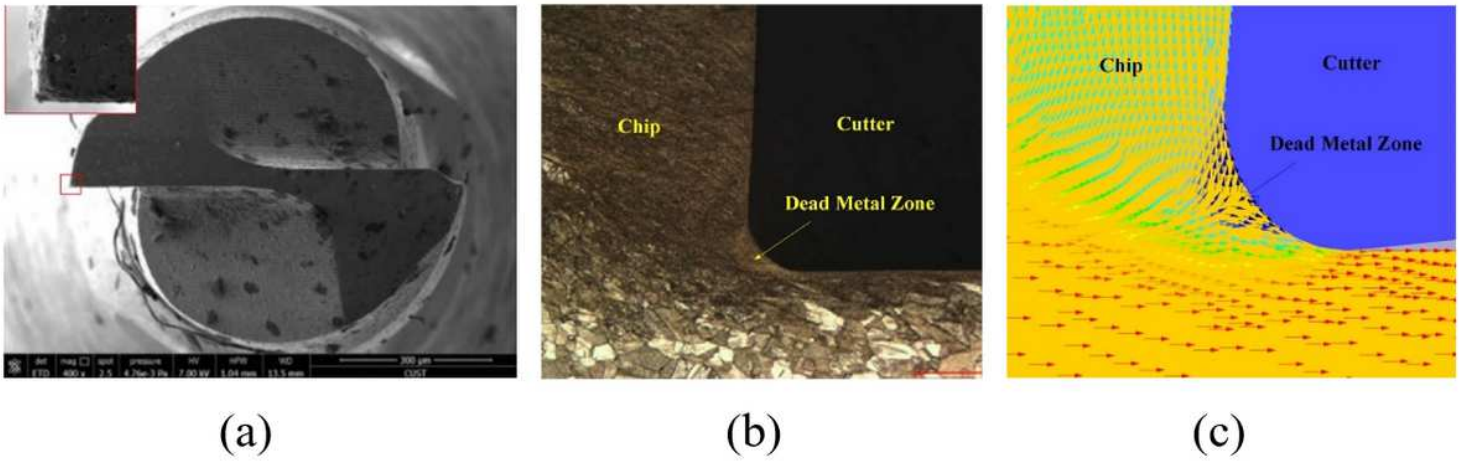

Figure 1

(a) SEM of the tool tip [2]. (b) DMZ experimentally observed by Ozturk and Altan [4]. (c) DMZ simulated by the finite element with the diagrams of material flow velocity vector [3].

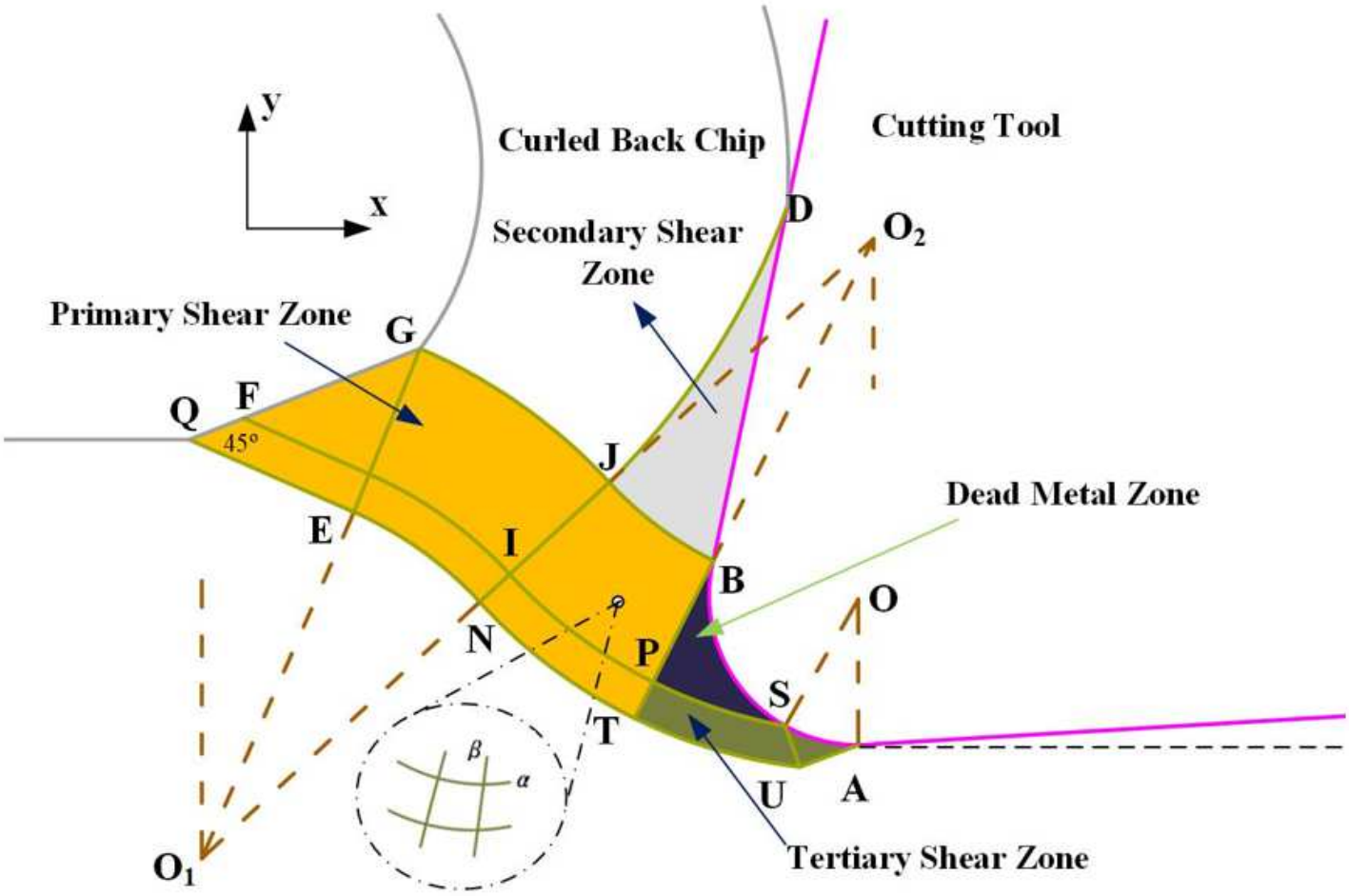

Figure 2

Diagrams of slip line field for metal orthogonal micro-cutting

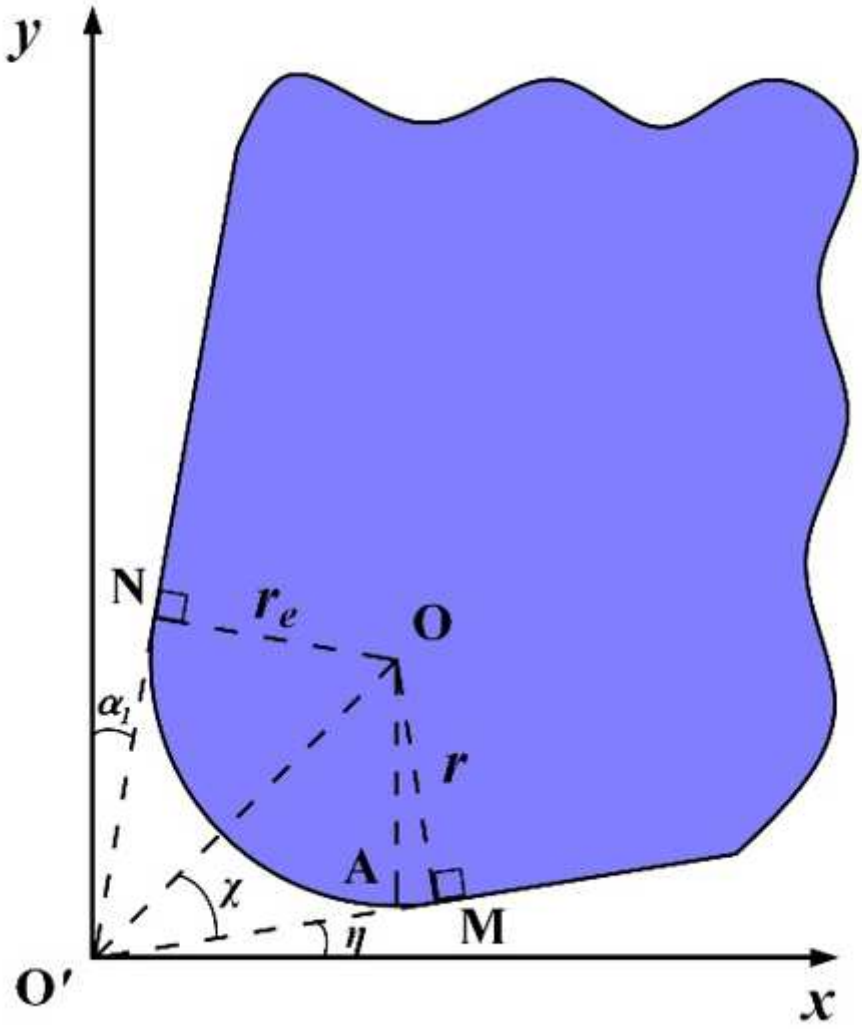

Figure 3

The rounded tool edge in the coordinate system.

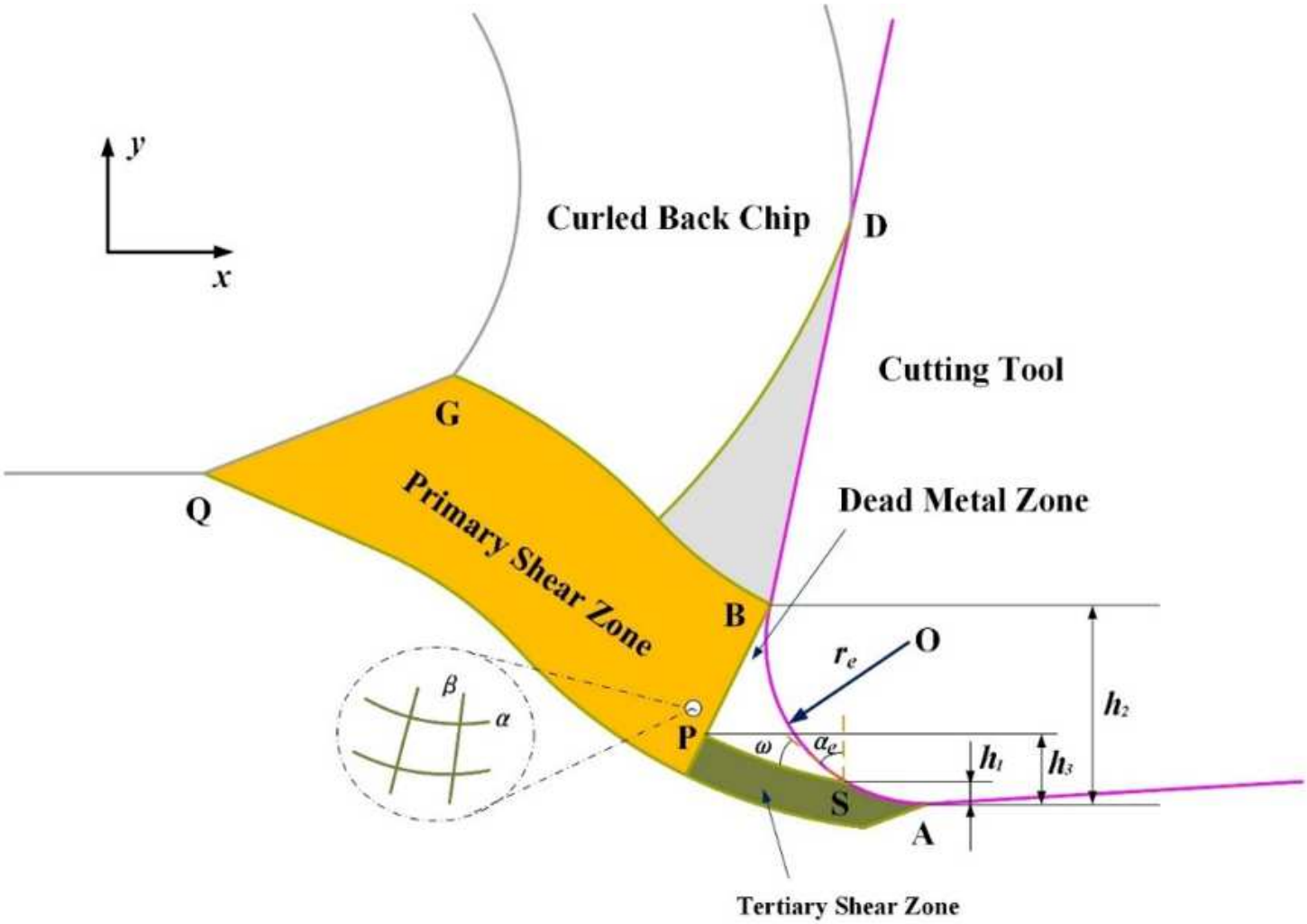

Figure 4

Geometry of the DMZ

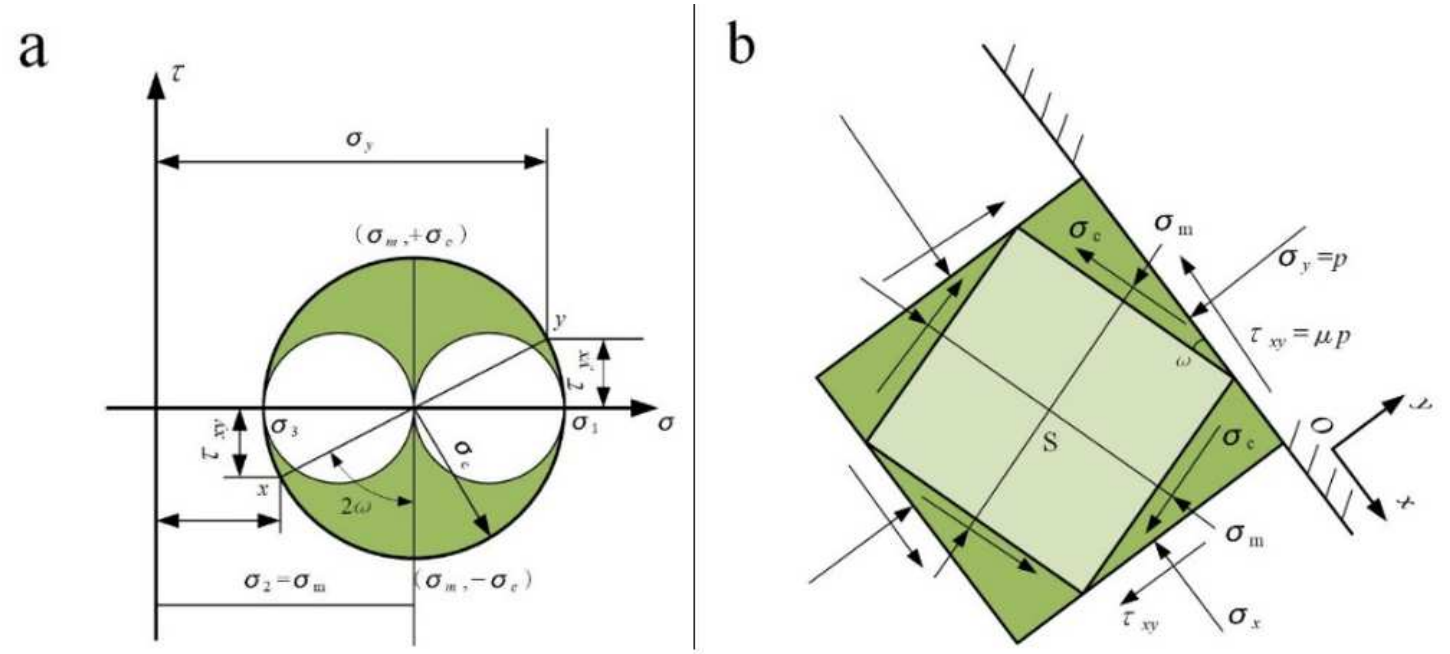

Figure 5

(a) Mohr circle of stress (b) Stress conditions at S point

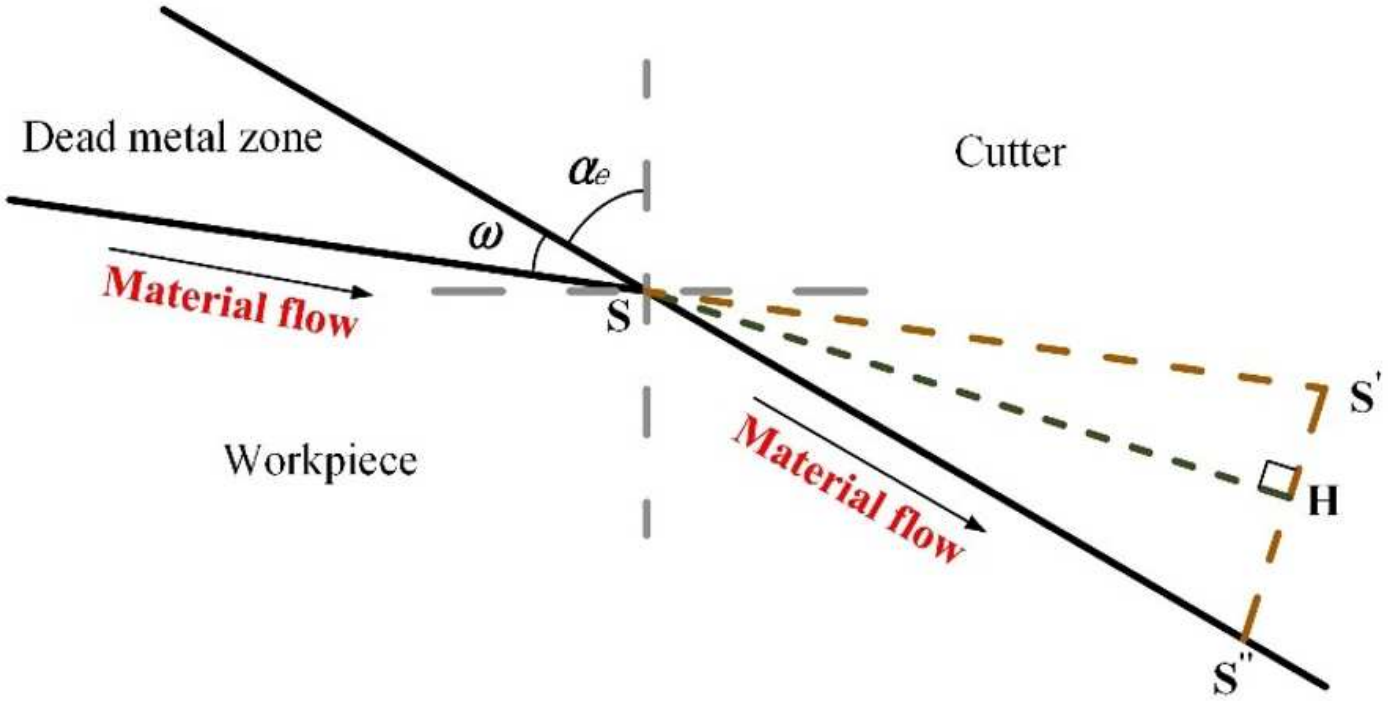

Figure 6

Strain diagram of separation point S.

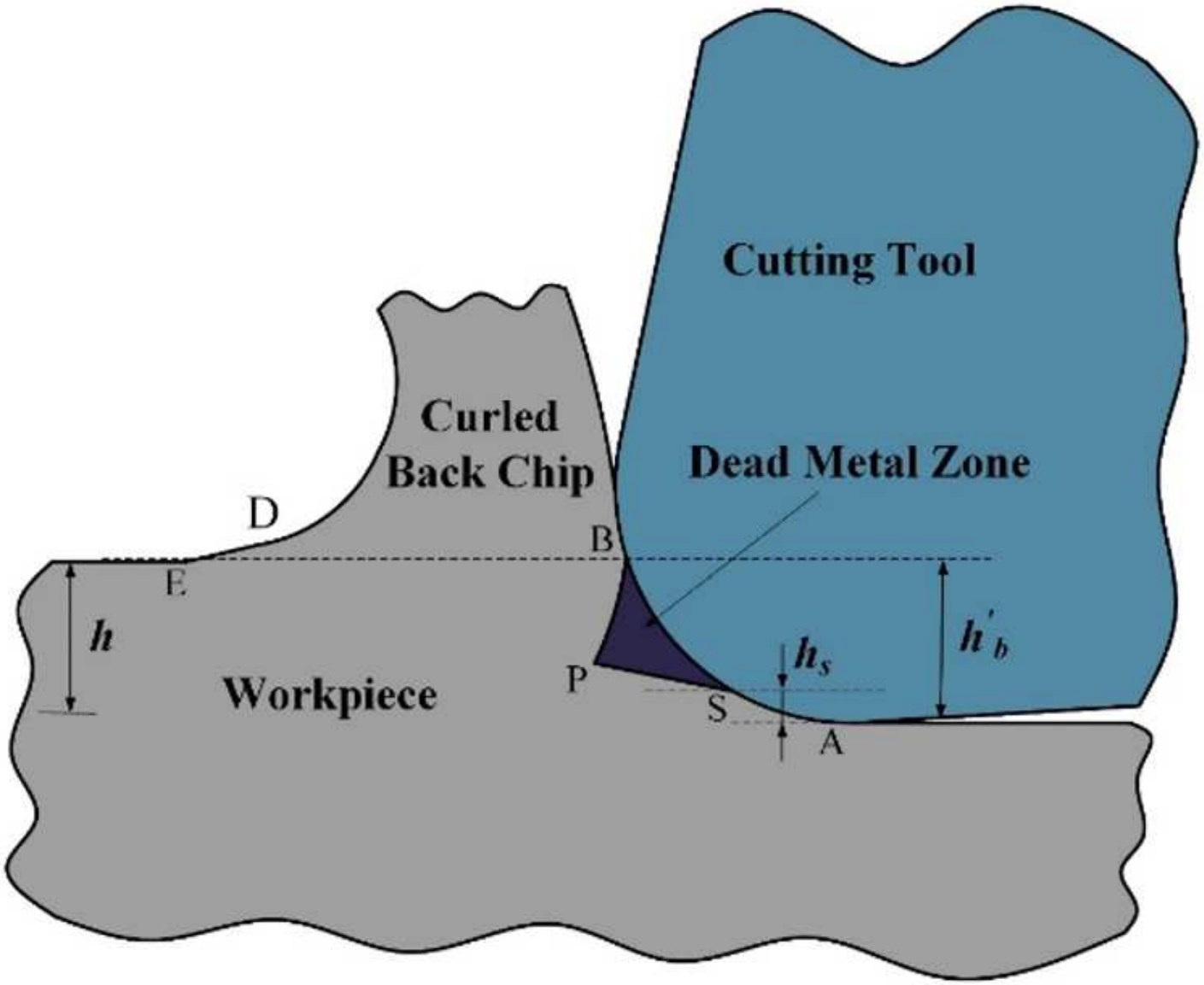

Figure 7

Cutting state diagram when h1<h<h2

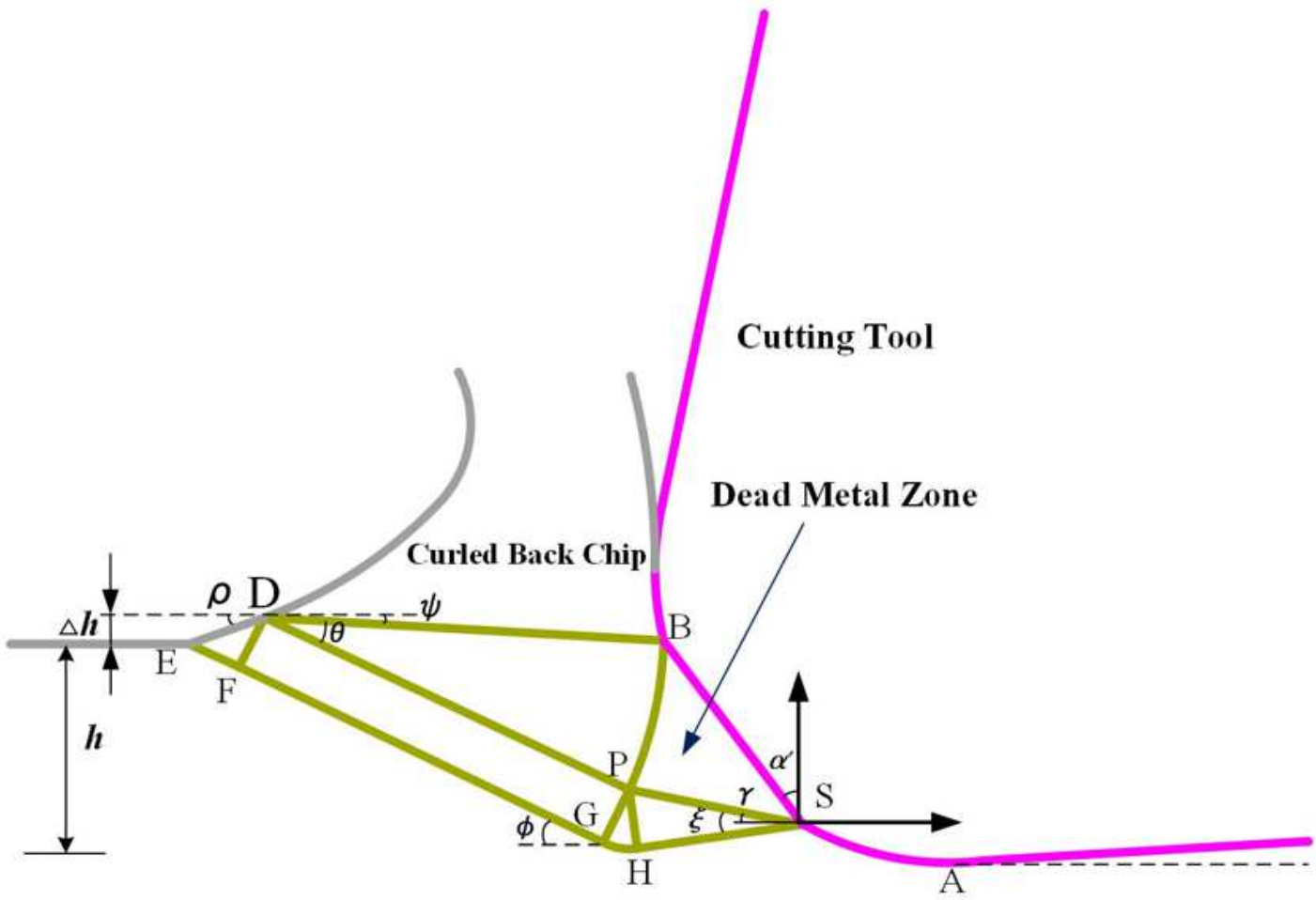

Figure 8

Schematic diagram of improved slip line field model with chamfering tool

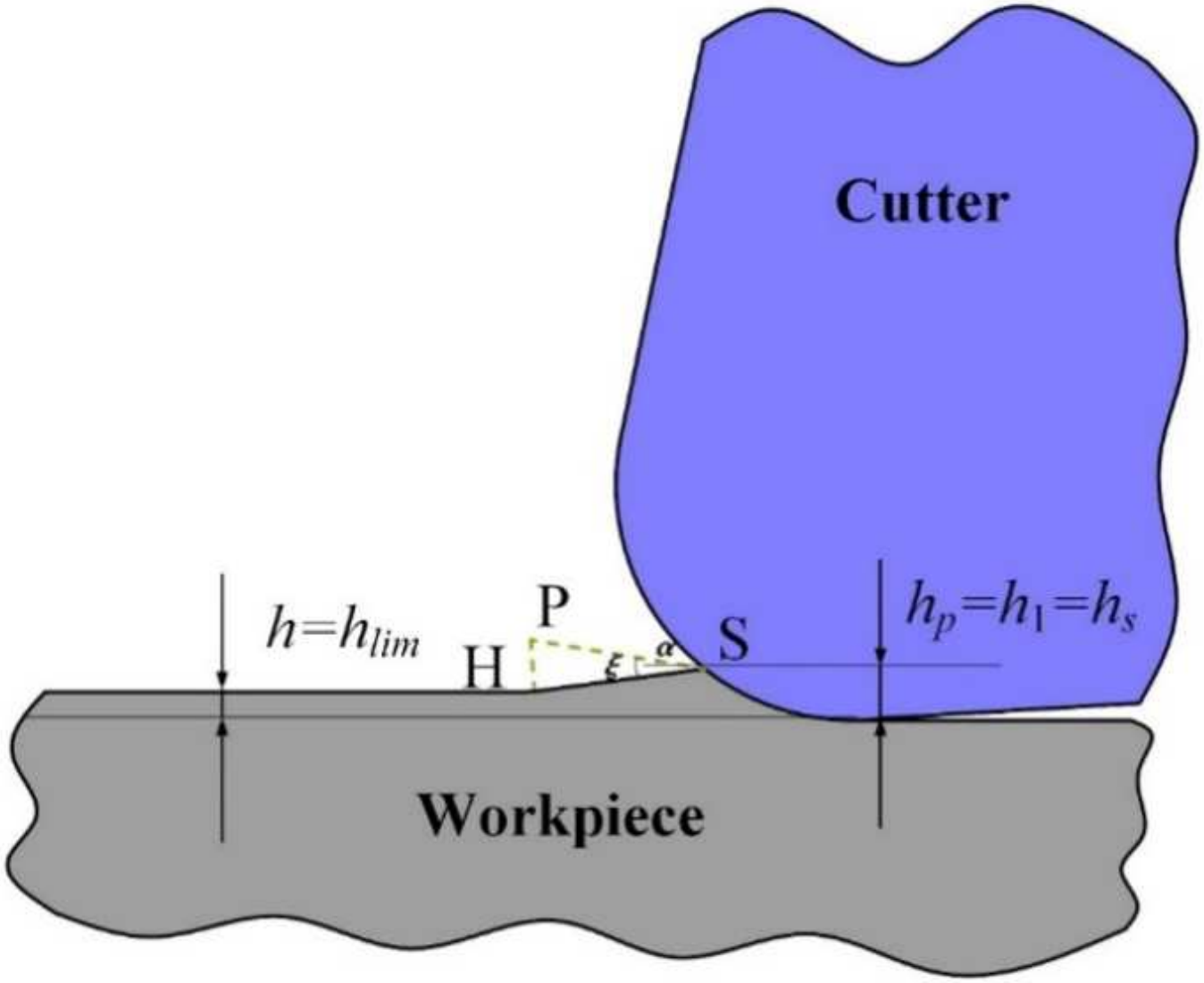

Figure 9

Cutting diagram with cutting depth h = hlim

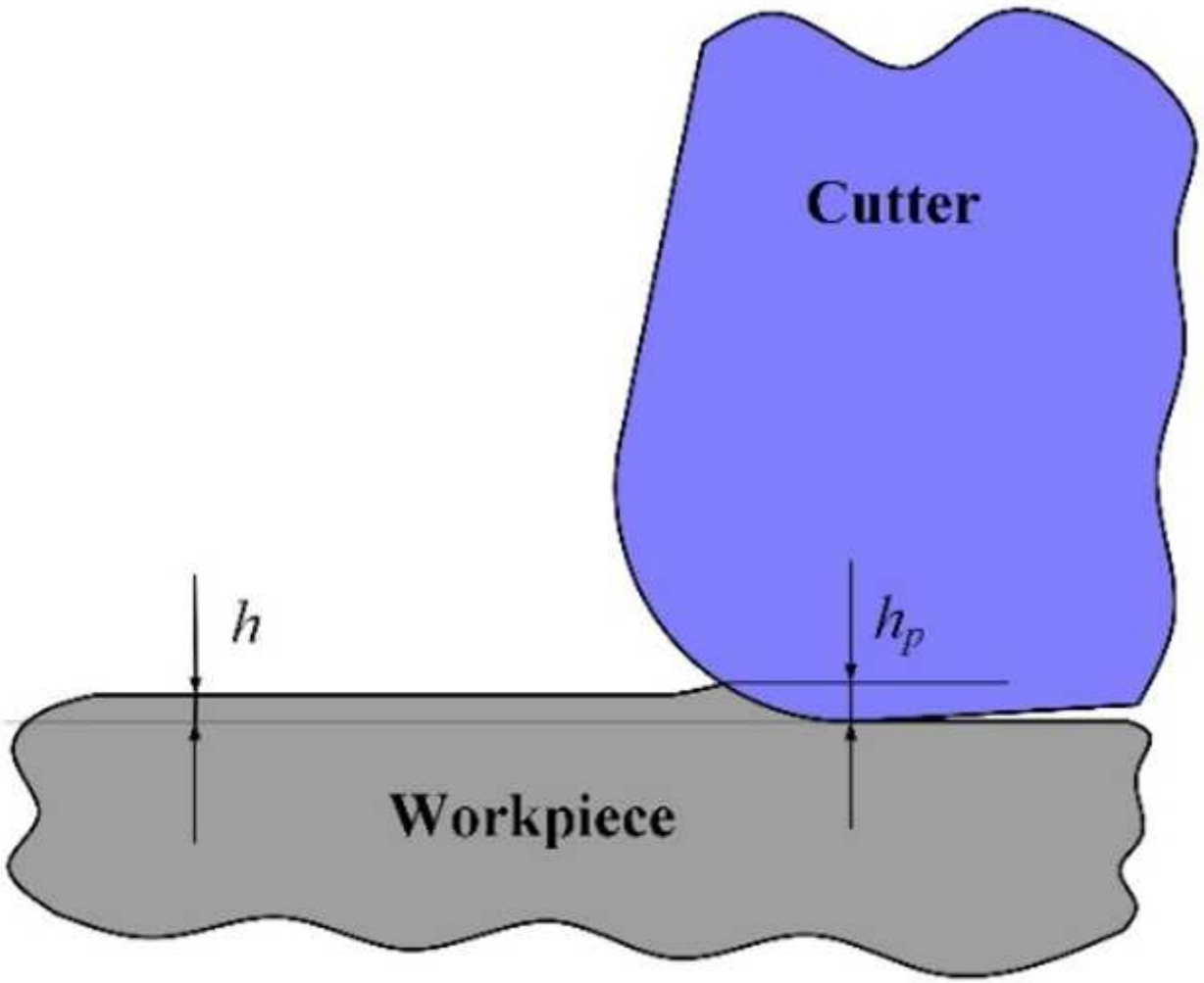

Figure 10

Cutting diagram with depth of cut h<hlim

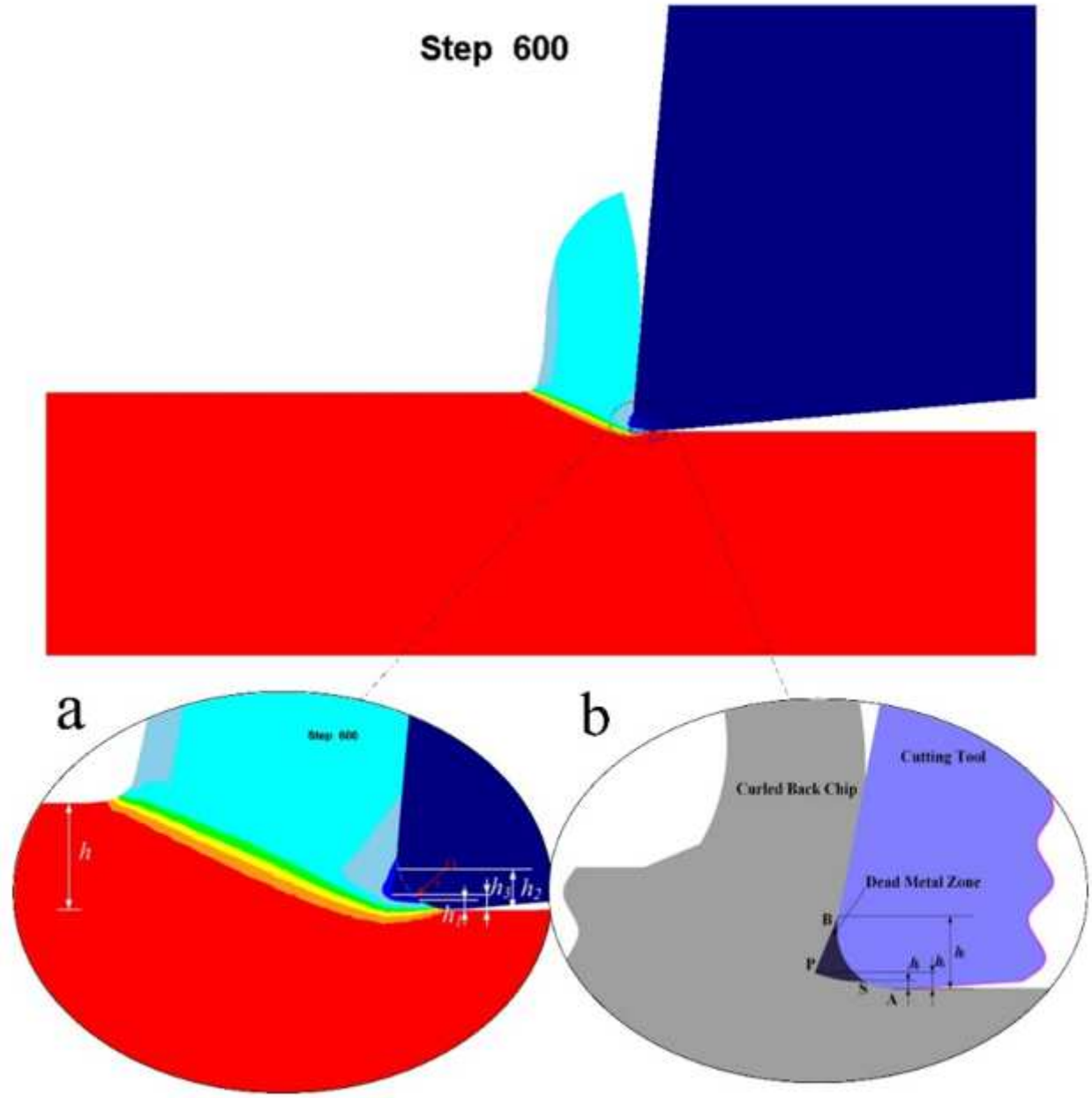

Figure 11

Three vertices height of simulated DMZ (a) Simulation diagram (b) Theoretical diagram

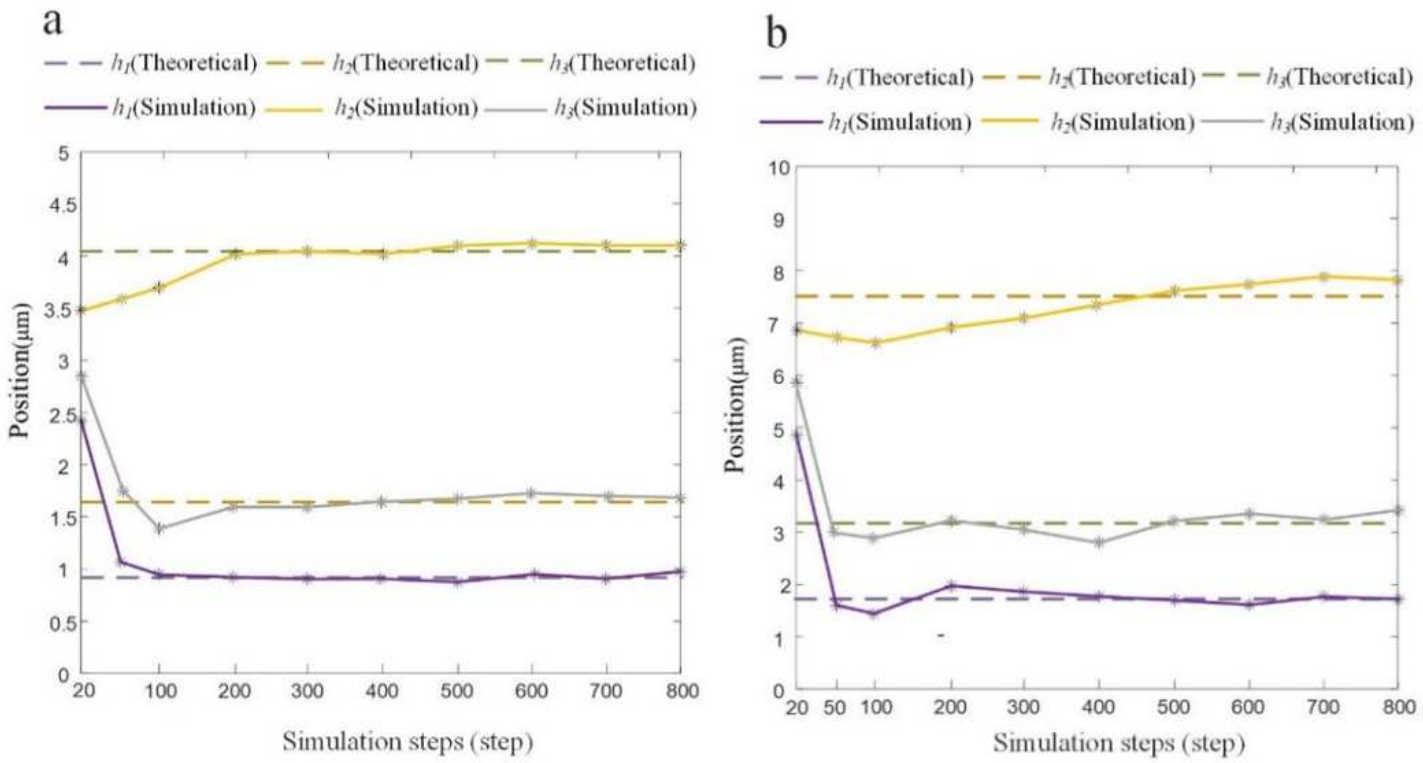

Figure 12

Comparison height acquired for separation points' by simulation with that of theoretically predicted under the condition at (a) re = 5 μm and (b) re= 8 μm.

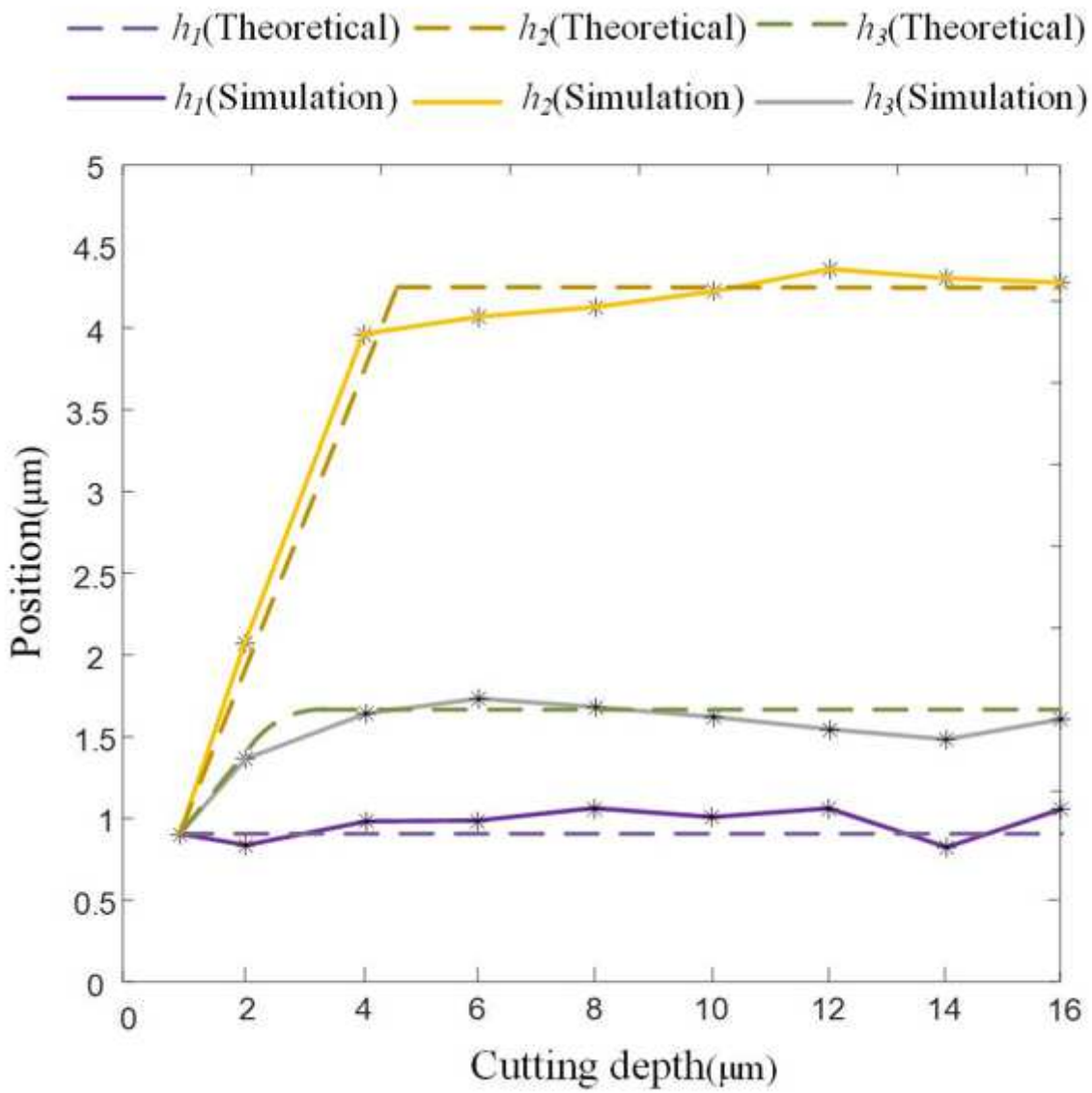

Figure 13

Comparison height acquired for separation points' by simulation with that of theoretically predicted at different uncut chip thickness with re = 5 μm

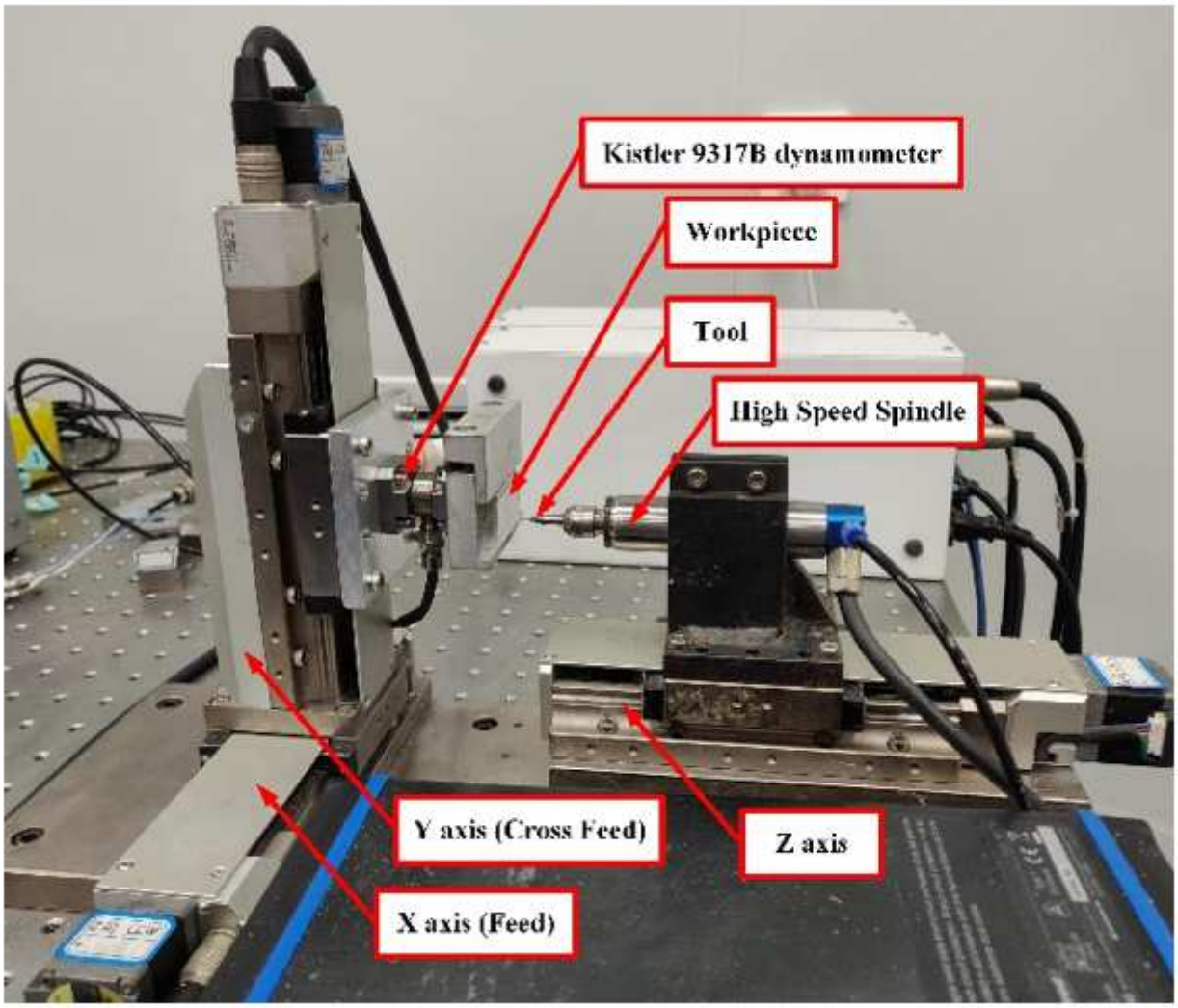

Figure 14

the 3-axis micromachining center

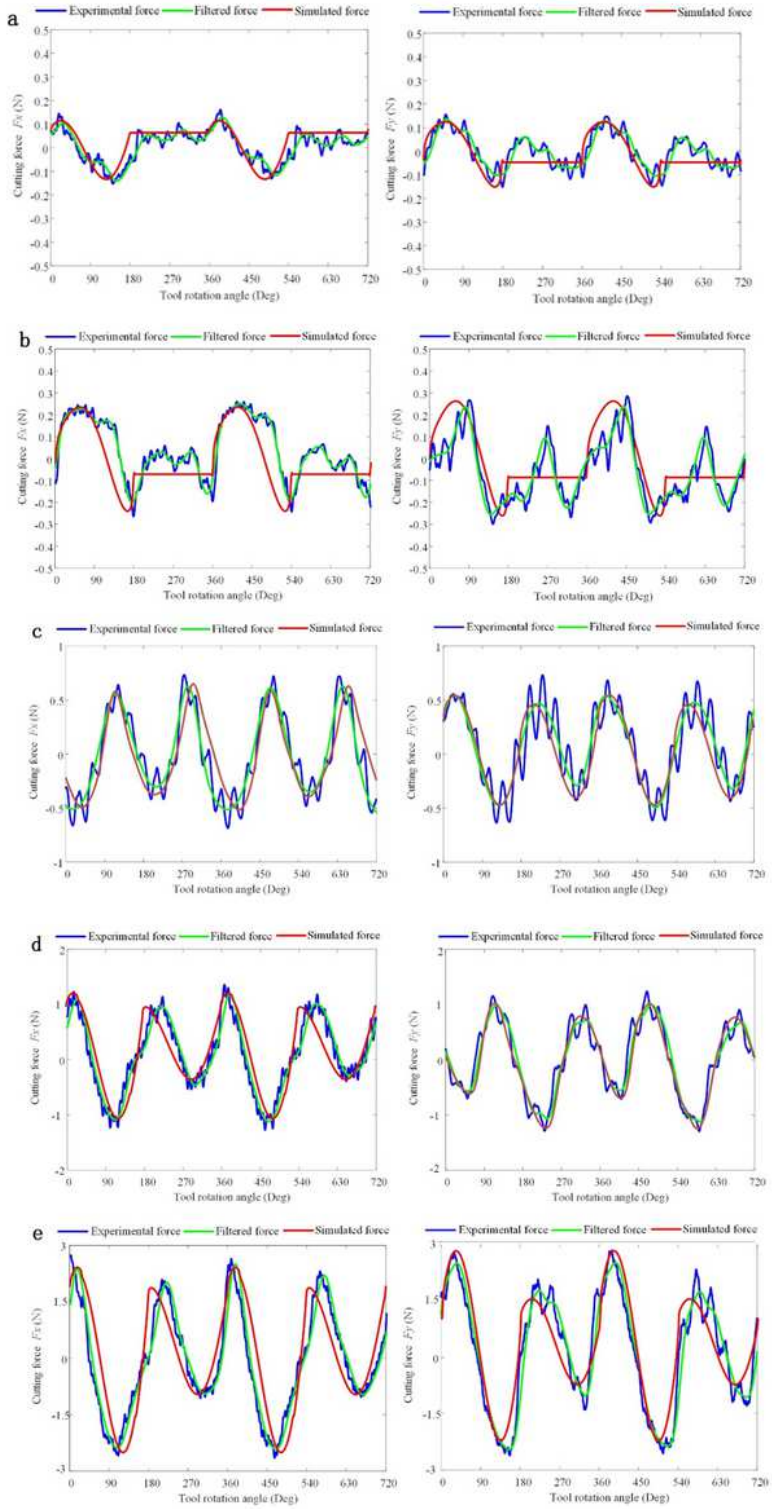

Figure 15

Comparison cutting force predicted with that of measured in micro/macro milling process (a) Test 1, (b) Test 2, (c) Test 3, (d) Test 4, (e) Test 5.